CHAPTER 20

Fundamentals of Pulse Compression Waveforms

Byron Murray Keel

Chapter Outline

20.1 INTRODUCTION

A radar system employing a continuous wave (CW) pulse exhibits a range resolution and signal-to-noise ratio (SNR) that are both proportional to pulse width. SNR drives detection performance and measurement accuracy and is a function of the energy in the pulse. Energy and SNR are increased by lengthening the pulse. Range resolution defines a radar's ability to separate returns in range and is improved by decreasing the pulse width. An undesired relationship, coupled through the pulse width, exists between the energy in a CW pulse and the pulse's range resolution. Near the end of World War II, radar engineers applied intrapulse modulation to decouple the two quantities. Range resolution was shown to be inversely proportional to bandwidth. A waveform's bandwidth could be increased via modulation, achieving finer range resolution without shortening the pulse. Waveforms that decouple resolution and energy via intrapulse or interpulse modulation are termed *pulse compression* waveforms.

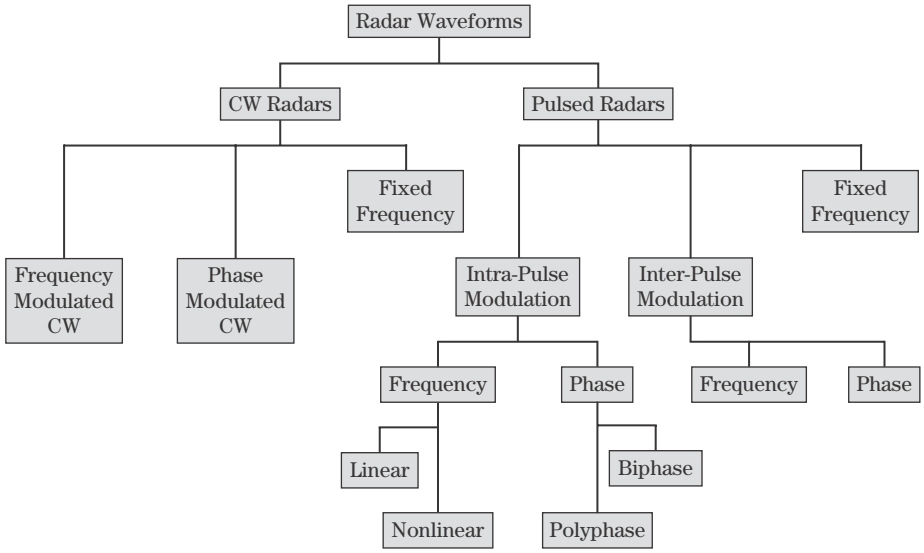

FIGURE 20-1 ■ Modern radars select from and employ many waveform modulations.

Modern radar systems employ both phase and frequency modulated waveforms. Waveform design takes into account a number of system requirements and constraints including percent bandwidth, sampling rate, dispersion, blind range, duty cycle, power, Doppler tolerance, and sidelobes as well as range resolution and SNR. A variety of waveform modulations have been developed since the 1950s to address these and other system requirements. Figure 20-1 contains a chart summarizing the various waveform modulations used in modern CW and pulsed systems.

This introductory chapter on pulse compression focuses on intrapulse linear frequency modulation and phase coding. The matched filter and resolution metrics are developed first. Pulse compression waveforms are then defined, and an overview of amplitude, phase, and frequency modulation is presented. The linear frequency modulated (LFM) waveform is explored in depth and serves as a basis for introducing a number of general concepts and properties including resolution, sidelobes, ambiguity surfaces, and processing gain. The properties of a CW pulse are examined and contrasted with the performance of pulse compression waveforms. In the latter sections, both biphase and polyphase codes are investigated. Special attention is paid to Barker codes, minimum peak sidelobe (MPS) codes, maximal length sequences, and Frank, P1, P2, P3, and P4 codes. The "Further Reading" section provides references to other frequency modulated (FM) waveforms and techniques (e.g., nonlinear FM, stepped frequency, stepped chirp, stretch processing) and phase codes (e.g., quadriphase codes).

20.2 | MATCHED FILTERS

In a radar system, a filter is applied to the received signal to maximize SNR at a point in time corresponding to the delay to the target. The filter maximizing SNR is derived from the transmit waveform and is termed a *matched filter.* A number of radar performance metrics, including range resolution, are defined in terms of the waveform's filtered response. The matched filter also plays an important role in processing pulse compression waveforms. The matched filter and its properties are examined in the following sections.

20.2.1 Relevance of SNR to Radar Performance

The probability of detecting a target and the accuracy of a measurement are both functions of signal-to-noise ratio. At the output of a square law detector, the probability of detecting a Swerling I or II target employing a single or multiple, coherently combined, pulses in the presence of additive, Gaussian distributed noise is [1]

$$P_D = (P_{FA})^{1/(1+SNR)} \tag{20.1}$$

where P_D is the probability of detection and P_{FA} is the probability of false alarm (see Chapters 2 and 15). For a fixed P_{FA}, detection performance improves with increasing SNR. The Cramèr-Rao bound defines the lower limit on accuracy with which the range to a target with known velocity may be measured and is given by [2]

$$\sigma_R = \frac{c}{4\pi B_{rms}} \frac{1}{\sqrt{SNR}} \tag{20.2}$$

where σ_R is the standard deviation in the range measurement, c is the speed of light ($\approx 3 \times 10^8$ m/sec), and B_{rms} is the root mean square (rms) waveform bandwidth with units of hertz. Cramèr-Rao lower bounds also exist for amplitude, Doppler, and angle measurements [2] (see Chapter 18). In general, the accuracy of a measurement is inversely proportional to the square root of SNR. Given the dependence of measurement accuracy and detection performance on SNR, radar systems are designed to maximize this quantity.

20.2.2 Energy Form of the Radar Range Equation

The radar range equation relates SNR to system and target parameters. A common form of the radar range equation, similar to the form in equation (2.11), is

$$SNR = \frac{P_t G_t G_r \lambda^2 \sigma}{(4\pi)^3 R^4 k T_s B L_s} \tag{20.3}$$

where P_t is the peak transmit power, G_t and G_r are the transmit and receive antenna gains, respectively, λ is the transmit wavelength, σ is the target radar cross-section (RCS), R is the one-way radial range to the target, k is Boltzman's constant ($k \approx 1.38 \times 10^{-23}$ W/Hz/K), T_s is the system noise temperature, B is the receiver noise bandwidth in hertz, and L_s is the aggregate system loss. In general, the receiver bandwidth is matched to the pulse bandwidth.

The bandwidth in hertz, B, of an unmodulated pulse of duration τ is commonly defined as the reciprocal of the pulse width. The terms *unmodulated* or *simple* pulse in this text refer to a real, rectangular-shaped pulse whose symmetric spectrum is centered at baseband (i.e., zero hertz). The spectrum $X(\omega)$ of a unit amplitude, unmodulated pulse with duration τ is a sinc function defined by

$$X(\omega) = \frac{\tau \sin\left(\frac{\omega\tau}{2}\right)}{\frac{\omega\tau}{2}} \tag{20.4}$$

where ω represents frequency in units of radians per second. The spectrum bandwidth in hertz, defined at the -4 dB width, equals the reciprocal of the pulse width.

In a radar system, the receiver bandwidth is matched to the waveform bandwidth to maximize SNR. Substituting the reciprocal of the pulse width for the receiver bandwidth, the radar range equation in equation (20.3) takes the form

$$SNR = \frac{P_t \tau G_t G_r \lambda^2 \sigma}{(4\pi)^3 R^4 k T_s L_s} \tag{20.5}$$

The product of peak power and pulse width defines the energy, E, in a pulse or

$$E = P_t \tau \tag{20.6}$$

and is the first term in the numerator of equation (20.5). The radar range equation in (20.5) is known as the energy form of the equation.

In a radar system, peak power is limited, and the transmitter may be operated in saturation to maximize energy on target. Lengthening a pulse increases the energy in the pulse and is a simple and cost-effective method for improving SNR. Modern radars employ different pulse widths chosen by the radar designer to support various operating modes.

20.2.3 The Form of the Matched Filter

In a radar system, the received waveform is filtered to maximize SNR at a time delay corresponding to the target's range. For an arbitrary waveform, $x(t)$, defined over the time interval $0 \leq t \leq \tau$, and embedded in additive white noise, the filter that maximizes SNR takes the form [3–7]

$$h(t) = ax^*(-t) \quad -\tau \leq t \leq 0 \tag{20.7}$$

and is referred to as the *matched filter*. The impulse response of the matched filter is a time-reversed and complex conjugated form of the transmit waveform, scaled by an arbitrary constant a, which is commonly set to 1. The form of the matched filter is advantageous since in a radar system the transmit waveform is known a priori, and thus the filter is known.

On receive, the matched filter $h(t)$ is convolved with the received waveform $x_r(t)$ to yield the output $y(t)$, or

$$y(t) = \int x_r(\alpha) h(t - \alpha) d\alpha \tag{20.8}$$

where α is a dummy variable of integration. Substituting (20.7) into (20.8) yields

$$y(t) = \int x_r(\alpha) x^*(\alpha - t) d\alpha \tag{20.9}$$

Applying the matched filter in (20.8) is equivalent to correlating the received signal with a copy of the transmit waveform as shown in (20.9). In most modern radars, the correlation is performed at baseband, after removal of the transmit radio frequency (RF) and receiver intermediate frequencies (IFs).

20.2.4 Point Target Model

A point target is defined as a scatterer with infinitesimal spatial extent. Some reflectors, such as a flat plate, sphere, dihedral, or trihedral, exhibit a response in range similar to a

point target. The mathematical model for the reflectivity of a point target with unit RCS, located at a slant range R from the radar, is the Dirac delta function, $\delta_D(t - 2R/c)$.

The waveform reflected off a point target and received at the radar at time delay t_d is modeled as

$$x_r(t) = b\exp(j\phi)x(t - t_d) \quad t_d \le t \le (t_d + \tau) \tag{20.10}$$

where b is a constant proportional to the received voltage, and ϕ is the phase measured by the coherent detector. The measured phase is a function of the transmit frequency and the slant range to the scatterer, or

$$\phi = -2\pi f\frac{2R}{c} = -\frac{4\pi R}{\lambda} \tag{20.11}$$

where f is the transmit center frequency, and $R = ct_d/2$. The received waveform in equation (20.10) is an amplitude-scaled and time-delayed version of the transmit waveform. The model of the received waveform in (20.10) does not account for dispersive (i.e., frequency-dependent) distortions or Doppler shifts due to relative motion. The impact of Doppler is addressed in subsequent sections. A point target is used throughout the chapter to examine properties of the matched filter and range resolution.

20.2.5 Match Filtered Response Proportional to Waveform Energy

The radar range equation defines SNR at the output of a matched filter, and the form of equations (20.5) and (20.6) states that SNR is proportional to the waveform's energy. Thus, the energy in the transmit pulse should appear as a scale factor at the output of the matched filter. This relationship is now examined.

Applying the matched filter to the target return in equation (20.10) yields

$$y(t) = \int be^{j\phi}x(\alpha - t_d)x^*(\alpha - t)d\alpha \tag{20.12}$$

By design, the output SNR is maximized at $t = t_d$. The output of the filter at time delay t_d is

$$y(t_d) = be^{j\phi}\int_{t_d}^{t_d+\tau}|x(\alpha - t_d)|^2 d\alpha \tag{20.13}$$

The output at $t = t_d$ is proportional to the energy in the transmit pulse, which is defined as

$$E = \int_0^{\tau}|x(t)|^2 dt \tag{20.14}$$

Substituting (20.14) into (20.13) yields

$$y(t_d) = be^{j\phi}E \tag{20.15}$$

The preceding equations (20.12) through (20.15) show that the matched filter takes a scalar multiple of the energy in the waveform and positions it at a time delay associated with the

point target. The relationship between the matched filter and the radar range equation is examined further in Section 20.2.8.

20.2.6 Fourier Relationships and the Matched Filter

The shape of the waveform spectrum, having applied the matched filter, establishes the shape of the time-domain response, and the duality between the two domains may be exploited to ascertain or influence the response. Given $x(t)$, the spectrum of the waveform is defined via the Fourier transform as

$$X(\omega) = \int x(t) \exp(-j\omega t) dt \equiv \Im\{x(t)\} \tag{20.16}$$

It is easy to show that the spectrum $H(\omega)$ of the matched filter [6,7] in equation (20.7) is

$$H(\omega) = X^*(\omega) \tag{20.17}$$

The filter spectrum in (20.17) is equal to the complex conjugate of the waveform's spectrum; thus, the filter is viewed as being "matched" in both the time and frequency domains.

Exploiting the duality between the time and frequency domains, the filtered output in (20.12) may be expressed in terms of its spectral components as

$$y(t) = \frac{1}{2\pi} \int b \exp(j\phi) X(\omega) \exp(-j\omega t_d) X^*(\omega) \exp(j\omega t) d\omega \tag{20.18}$$

An examination of the terms comprising equation (20.18) is instructive. The Fourier transform of the time-delayed and amplitude-scaled received signal in (20.10) is

$$\Im\{b \exp(j\phi) x(t - t_d)\} = b \exp(j\phi) X(\omega) \exp(-j\omega t_d) \tag{20.19}$$

The right side of (20.19) contains the first four terms inside the integral in equation (20.18). Time delay produces a linear phase ramp across the spectrum with a slope determined by the delay. The other terms in (20.18) include the waveform's spectrum $X(\omega)$, the matched filter's spectrum $X^*(\omega)$, and the Fourier kernel $\exp(j\omega t)$ associated with the inverse transform.

Grouping terms, (20.18) may be written as

$$y(t) = \frac{b \exp(j\phi)}{2\pi} \int |X(\omega)|^2 \exp(-j\omega t_d) \exp(j\omega t) d\omega \tag{20.20}$$

The factors in (20.20) determine both the shape and location of the filtered response in the time domain. The product of the signal and matched filter spectra produces a squared magnitude response. The waveform's phase in the frequency domain has been removed by the filter. The shape of the squared magnitude response defines the time-domain response via Fourier transform pairs and may be intentionally modified or chosen to achieve a desired response. For example, spectral shaping is exploited in both linear and nonlinear frequency modulated waveforms to achieve low-range sidelobes [2,4,7]. The linear phase term contains the time-delay information and is responsible for positioning the filtered response in the time domain.

The response associated with N_{pt} point targets or scatterers may be modeled as

$$y(t) = \frac{1}{2\pi} \int |X(\omega)|^2 \left[\sum_{i=1}^{N_{pt}} b_i \exp(j\phi_i) \exp(-j\omega t_{d_i}) \right] \exp(j\omega t) d\omega \tag{20.21}$$

where b_i, t_{d_i}, and ϕ_i are the amplitude, time delay, and phase associated with the i-th point target, respectively.

20.2.7 Derivation of the Matched Filter

Having examined Fourier relationships between the time and frequency domains, the derivation of the matched filter is relatively straightforward. The approach taken is similar to that found in [8]. Consider applying an arbitrary filter $H(\omega)$ to the return from a point target. The filtered signal is

$$y(t) = \frac{1}{2\pi} \int b \exp(j\phi) X(\omega) \exp(-j\omega t_d) H(\omega) \exp(j\omega t) d\omega \tag{20.22}$$

where $b \exp(j\phi) X(\omega) \exp(-j\omega t_d)$ is the spectrum of the return from a point target located at time delay t_d, b is the amplitude of the return, and ϕ is the measured phase.

The received signal is competing with thermal noise in the receiver. The two-sided power spectrum associated with white noise is defined as

$$N(\omega) = N_0 \tag{20.23}$$

where N_0 has units of watts per hertz. The term *white noise* means that the noise is uncorrelated, yielding a power spectrum that is constant over frequency. Applying an arbitrary filter $H(\omega)$ to white noise yields an expected output power given by

$$\overline{n^2(t)} = \frac{N_0}{2\pi} \int |H(\omega)|^2 \, d\omega \tag{20.24}$$

where $n(t)$ is a realization of the noise as a function of time. $n(t)$ is a voltage, so squaring the realization yields the instantaneous noise power. The overbar denotes the expected value, $\overline{n^2(t)} = \mathrm{E}\{n^2(t)\}$ where E{ } is the expectation operator. The noise in a receiver channel is assumed to be Gaussian distributed with zero mean. Equation (20.24) thus represents the average noise power (or equivalently the variance of the noise) at the output of the filter.

For a target, the output of the filter in equation (20.22) at time delay t_d is

$$y(t_d) = \frac{b \exp(j\phi)}{2\pi} \int X(\omega) H(\omega) \, d\omega \tag{20.25}$$

and represents a voltage. The squared magnitude defines the power or

$$|y(t_d)|^2 = \left| \frac{b}{2\pi} \int X(\omega) H(\omega) \, d\omega \right|^2 \tag{20.26}$$

The signal-to-noise ratio at the output of the filter at time delay t_d is

$$SNR = \frac{|y(t_d)|^2}{\overline{n^2(t)}} \tag{20.27}$$

or

$$SNR = \frac{b^2 \left| \int X(\omega) H(\omega) d\omega \right|^2}{2\pi N_0 \int |H(\omega)|^2 d\omega} \tag{20.28}$$

The objective is to define a filter $H(\omega)$ that maximizes SNR. The Schwartz inequality may be applied to the numerator in equation (20.28). The Schwartz inequality states that, for any $X(\omega)$ and $H(\omega)$,

$$\left| \int X(\omega) H(\omega) d\omega \right|^2 \leq \int |X(\omega)|^2 d\omega \int |H(\omega)|^2 d\omega \tag{20.29}$$

For the equality to hold, the filter must be of the form

$$H(\omega) = aX^*(\omega) \tag{20.30}$$

where a is an arbitrary constant. Equation (20.30) defines the spectrum of the filter that maximizes the SNR at a time delay corresponding to the target's range. The impulse response in the time domain is obtained via the inverse Fourier transform applied to equation (20.30) and is

$$h(t) = ax^*(-t) \tag{20.31}$$

which is a time-reversed and complex conjugated copy of the transmit waveform and is equivalent to the filter previously defined in equation (20.7).

20.2.8 The Radar Range Equation and Matched Filter Relationship

The relationship between the radar range equation and the matched filter is shown by substituting the matched filter in (20.30) into (20.28), yielding

$$SNR = \frac{b^2 \frac{1}{2\pi} \int |X(\omega)|^2 d\omega}{N_0} \tag{20.32}$$

Now, Parseval's theorem [9] states that energy in the time-domain signal must equal the energy in the frequency domain, or

$$\int_{-\infty}^{\infty} |x(t)|^2 dt = \frac{1}{2\pi} \int_{-\infty}^{\infty} |X(\omega)|^2 d\omega \tag{20.33}$$

Recognizing that the energy in the transmit waveform is defined by

$$E = \int_{-\infty}^{\infty} |x(t)|^2 dt \tag{20.34}$$

equation (20.32) may be written as

$$SNR = \frac{E}{N_0} b^2 \tag{20.35}$$

By selecting $b^2 = G_t G_r \lambda^2 \sigma / (4\pi)^3 R^4 L_s$ and noting that $E = P_t \tau$ and $N_0 = kT_s$, it is evident that (20.35) is equivalent to the radar range equation (20.5); that is, both are of the form $SNR \propto E/N_0$.

20.2.9 The Match Filtered Response for a Simple Pulse

A simple (or CW) pulse is applied in many radar systems, and therefore an examination of its properties and its match filtered response is worthwhile and will provide the motivation for pulse compression waveforms. Consider a simple pulse with constant amplitude, A, and pulse width, τ, defined by

$$x(t) = A, \quad -\frac{\tau}{2} \le t \le \frac{\tau}{2} \tag{20.36}$$

and the corresponding matched filter, obtained from equation (20.7) with $a = 1$,

$$h(t) = A, \quad -\frac{\tau}{2} \le t \le \frac{\tau}{2} \tag{20.37}$$

The filtered response is a triangle defined by

$$y(t) = \begin{cases} A^2(t+\tau), & -\tau \le t \le 0 \\ A^2(\tau - t), & 0 < t \le \tau \end{cases} \tag{20.38}$$

and is depicted in Figure 20-2. Note that the length of the filtered response is equal to twice the original pulse width. The expansion is a property of the filtering operation. For any finite duration waveform, the match filtered output exhibits a response whose duration is equal to twice the original waveform extent. The filtered signal represents a voltage, and the instantaneous power is defined as the square of the voltage. The peak voltage is $A^2\tau$, which equals the energy in $x(t)$, consistent with equations (20.14) and (20.15).

In many instances, the rectangular pulse is a good first-order model that facilitates analysis. In an actual system, the ideal pulse is not realizable due to bandwidth limits imposed by the hardware. Band-limiting or shaping of the waveform's spectrum increases the pulse duration and prevents instantaneous rise and fall times at the pulse boundaries.

When employing a simple pulse, the low-pass filter on receive serves as an approximation to the matched filter. The bandwidth of the filter is matched to the pulse bandwidth, or, equivalently, the reciprocal of the pulse width. A loss in SNR occurs if the spectrum of the waveform and the filter are not matched exactly except for a linear phase term.

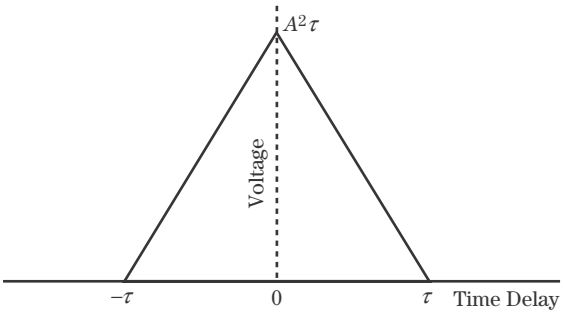

FIGURE 20-2 ■ The simple pulse of duration τ has a match filtered response of duration 2τ.

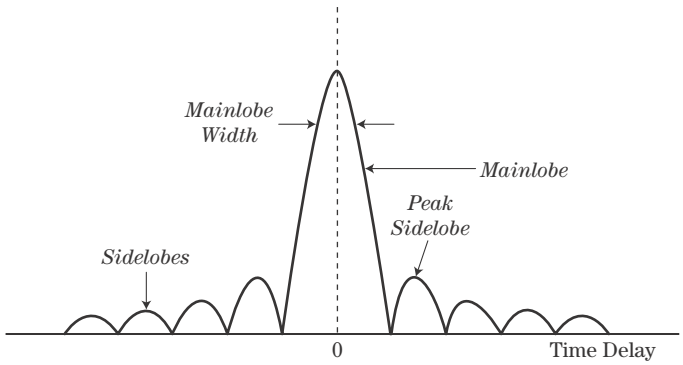

FIGURE 20-3 ■ A generic match filtered response includes the mainlobe and sidelobes.

20.2.10 Properties of the Match Filtered Response

Many waveform properties, including SNR, range resolution, and Doppler tolerance, are defined in terms of the match filtered response. In general, a waveform's filtered response exhibits both a mainlobe and sidelobe structure, as illustrated in Figure 20-3. The mainlobe is defined as the portion of the response positioned between the nulls that lie adjacent to the peak of the response, and the sidelobes are defined as the portion of the response outside the mainlobe. A simple, unmodulated pulse exhibits only a mainlobe.

With any waveform, SNR is maximized at the peak of the mainlobe. Points on the response that are located below the peak achieve a SNR that is less than the maximum. In a radar system, samples of the response do not always include the peak, and thus, the potential exists for a loss in SNR that must be accounted for in the design. The loss associated with not sampling the peak of the response is termed *straddle loss* (see Section 20.4).

Range resolution is a measure of the ability of a radar to distinguish between objects closely spaced in range and is defined in terms of the mainlobe width. A more formal definition and detailed examination of resolution is provided in subsequent sections.

Sidelobes are an undesired by-product of applying the matched filter to a modulated waveform. In the range dimension, sidelobes are interchangeably referred to as range or time sidelobes. Sidelobes are problematic because those associated with a large RCS target may be higher in amplitude than the mainlobe response of a weaker target and thus may mask the presence of the smaller target even when the two are well resolved in range. Sidelobe levels are commonly referenced relative to the peak of the mainlobe. Both peak and integrated sidelobe ratios are important performance metrics. Integrated sidelobe levels are relevant when operating in a distributed clutter environment, as the cumulative sidelobe contributions associated with clutter may degrade the quality of a target measurement. For example, integrated sidelobes contribute to the multiplicative noise in a synthetic aperture radar (SAR) image [10].

20.3 RANGE RESOLUTION

In many systems, an ability to resolve objects in range is required and is defined in terms of the radar's range resolution. Range resolution requirements vary depending on the application or radar mode. For example, search functions may employ a relatively coarse range resolution on the order of or greater than the target's physical extent. In contrast,

target recognition (i.e., classification or identification) requires a resolution sufficient to resolve individual scattering centers located along the target. Resolution requirements on the order of 0.5 to 1 foot may be required in some systems [11]. In track, resolution requirements may be finer than those used during search.

Ultimately, a radar's ability to resolve closely spaced objects is governed by the shape and width of the waveform's mainlobe response. Two of the more common width metrics [2,4,6] used to define resolution are:

1. The *Rayleigh criterion*, which defines resolution as the separation between the peak and the first null.
2. The mainlobe width at a specific point below the peak of the response, such as the -3 dB point.

Each metric is described in more detail in the following sections.

20.3.1 Resolution as Defined by the Rayleigh Criterion

The Rayleigh criterion states that two point targets are resolved when the targets are separated in range such that the peak of the match filtered response of one target falls on the first null of the second target. The targets are considered to be resolved since no energy from one target is present at, or is competing with, the peak of the second target's return.

The Rayleigh criterion may be applied to any waveform, including pulse compression waveforms exhibiting both a mainlobe and sidelobe response. The Rayleigh separation is illustrated in Figure 20-4 using a simple pulse. The peak of the response and the first null are separated by τ seconds. For a simple pulse, the null occurs when the filtered response goes to zero. Given a monostatic radar, time delay represents the total round-trip delay; thus, two point target returns separated by a τ second delay are separated in range by

$$\delta R = \frac{c\tau}{2} \tag{20.39}$$

where c is the speed light ($\approx 3 \times 10^8$ m/sec). Equation (20.39) represents the Rayleigh resolution associated with a simple, ideal pulse of duration τ. Given that the match filtered response for the simple pulse is a triangle (Figure 20-2), the amplitude is one-half the peak amplitude (-6 dB) at a delay of $\pm\tau/2$ seconds from the peak. Thus, for a simple pulse the Rayleigh resolution is equivalent to the -6 dB mainlobe width.

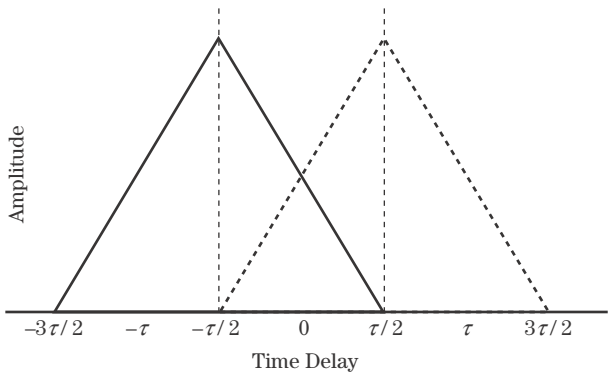

FIGURE 20-4 ■ Individual responses from two point targets separated by the Rayleigh resolution.

Some explanation is needed with regard to the terminology used to quantify resolution. The terms *improved* or *enhanced* resolution refer to a decrease in δR, while the terms *degraded* or *reduced* resolution refer to an increase in δR. Fine resolution implies relatively small values of δR, whereas coarse resolution implies relatively large values of δR. For a simple pulse, enhanced resolution is achieved by decreasing the pulse width.

20.3.2 Resolution Defined in Terms of Mainlobe Width

Range resolution may be defined with respect to the mainlobe width measured at a specified point below the peak. The -3 dB width is commonly used to define resolution and corresponds to the half-power point. In general, the physical separation associated with the -3 dB width is less than the separation associated with the Rayleigh resolution.

In some cases, several width metrics (e.g., -3, -6, -10, and -20 dB) may be employed to characterize the mainlobe width and roll-off. The shape of the mainlobe varies depending on the modulation employed and any weighting applied to suppress the range sidelobes. A single number is often used to quantify resolution, but depending on the application, a more detailed characterization of the mainlobe response may be required to fully assess performance.

20.3.3 Woodward's Range Resolution Constant

Woodward [2,4,5] describes a time resolution constant used to compare the range resolution of different waveforms. The metric defines a rectangle with peak amplitude and energy equal to that of the waveform's match filtered response. The width of such a rectangle is

$$T_{res} = \frac{\int_{-\infty}^{\infty} |y(t)|^2 dt}{|y(0)|^2} \tag{20.40}$$

Waveforms producing small values to T_{res} exhibit fine range resolution.

20.3.4 The Relationship between Bandwidth and Range Resolution

In Section 20.3.1, it was shown that for a simple pulse, range resolution is proportional to pulse width. This turns out to be a special case where pulse width and bandwidth are inversely related. In general, range resolution is inversely proportional to waveform bandwidth. This relationship is less intuitive but is demonstrated using the Fourier uncertainty principle.

The Fourier uncertainty principle [9] states that a signal's "width" in one domain is inversely proportional to the signal's "width" in the transform domain. The uncertainty principal uses second-order moments to define the width of a signal in the time domain as

$$D_t = \sqrt{\int_{-\infty}^{\infty} t^2 |y(t)|^2 dt} \tag{20.41}$$

and the signal's width in the frequency domain as

$$D_\omega = \sqrt{\int_{-\infty}^{\infty} \omega^2 |Y(\omega)|^2 d\omega} \tag{20.42}$$

where $y(t) \overset{\mathfrak{F}}{\longleftrightarrow} Y(\omega)$. Given that $y(t)$ is the output of the matched filter and $Y(\omega) = |X(\omega)|^2$, D_t is a measure of the width of the filtered time-domain response and D_ω is a measure of the power spectrum's width (or bandwidth). The Fourier uncertainty principle states that

$$D_t D_\omega \geq \sqrt{\frac{\pi}{2}} \tag{20.43}$$

which implies that the width of the time-domain response is inversely proportional to a measure of the waveform's bandwidth. The equality holds for Gaussian-shaped signals.

The inverse relationship between bandwidth and resolution applies to a simple pulse. As noted previously, the spectrum of a simple pulse is a sinc function with a -4 dB bandwidth defined by the inverse of the pulse width (i.e., $B = 1/\tau$). Substituting bandwidth for pulse width into equation (20.39) yields

$$\delta R = \frac{c}{2B} \tag{20.44}$$

For a simple pulse, equations (20.39) and (20.44) are equivalent definitions of resolution and correspond to the Rayleigh resolution or the -6 dB width.

Range resolution is commonly computed as

$$\delta R = \kappa \frac{c}{2B} \tag{20.45}$$

where B is the waveform bandwidth in hertz, and κ is scale factor used to account for intentional or unintentional factors that degrade resolution. The expression in (20.45) is not tied to a particular definition or measure of resolution (e.g., Rayleigh) or bandwidth. Instead, definitions of resolution and bandwidth and the scale factor κ are often chosen such that (20.45) holds. To fully assess "resolution," the entire mainlobe in terms of both width and roll-off must be characterized. In addition, the relative amplitude and phase difference between two scatterers also affects the shape of the combined response.

20.3.5 An Examination of Resolution Using Two Point Targets

For two closely spaced point targets, the shape of the composite response is a function of their separations, amplitudes, and phases. It is common to assume that if two scatterers are separated by the radar's "range resolution," then they are both visually distinguishable in range. This is not always the case. The metrics used to define resolution are not formulated to necessarily achieve a visually pleasing composite response in which the two scatterer returns are easily recognized.

Consider a simple pulse and two equal amplitude point targets separated in range by the Rayleigh resolution of $c\tau/2$ meters (τ seconds in time delay). The individual match filtered responses are depicted in Figure 20-4. The return from a point target produces a constant phase shift $\phi = -4\pi fR/c$ that is proportional to the range to the target and the radar's transmit center frequency. Two point scatterers separated in range by integer multiples of $\lambda/2$ exhibit a phase difference that is a multiple of 2π radians, equivalent to 0°,

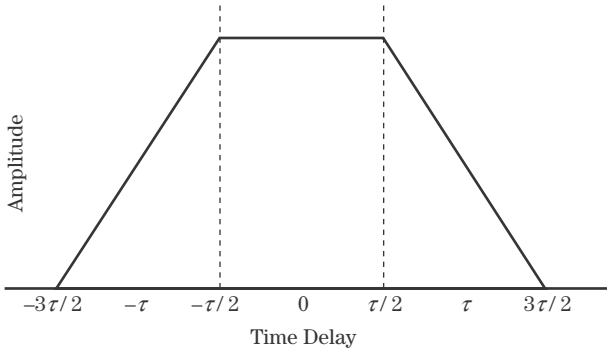

FIGURE 20-5 ■ Combined response for two point targets with phase difference equal to 0°.

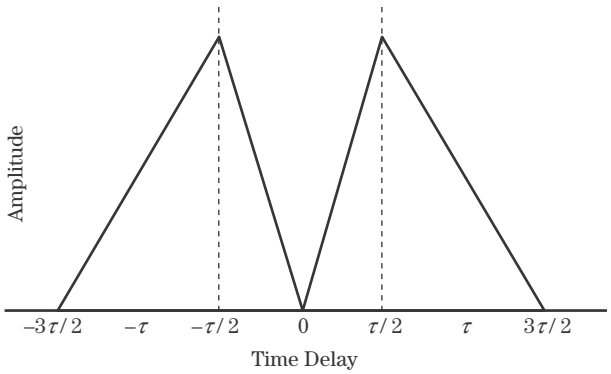

FIGURE 20-6 ■ Combined response for two point targets with phase difference equal to 180°.

while two scatterers separated in range by odd multiples of $\lambda/4$ exhibit a phase difference equivalent to 180°. If the target amplitudes are equal and the phase difference is 0°, the combined response is that shown in Figure 20-5. The composite response does not provide a visual indication that two targets are present, even though the targets are separated by the Rayleigh resolution. Next assume the same scatterer separation and a different transmit frequency. If the phase difference between the two scatterers is 180°, then the combined response is that shown in Figure 20-6. Visually, the response suggests the presence of two targets. In both instances, the targets are resolved based on the Rayleigh criterion. In general, commonly applied definitions of resolution do not take into account amplitude and phase differences or the shape of the composite response.

20.4 STRADDLE LOSS

In a modern radar, the received signal is sampled in time and processed digitally. A sampled, match filtered response exhibits a loss in SNR if the samples do not include the theoretical peak value. The loss in SNR is defined as the ratio of the square of the largest sampled value to the square of the theoretical peak value and is commonly referred to as *straddle loss*, indicative of the fact that the peak falls between two sample bins. The largest or peak straddle loss occurs when the peak of the response falls mid-way between 2 samples and is calculated as

$$L_{\text{st\_pk}} = 20\log_{10}\left|\frac{y(t)}{y(0)}\right|_{t=\Delta t/2} \tag{20.46}$$

where Δt is the time between samples, and the peak of the response occurs at $t = 0$. For a given waveform, straddle loss decreases with increasing sample rate. The peak straddle

loss associated with a simple pulse is −6 dB given a sample spacing equal to the pulse width (i.e., $\Delta t = \tau$).

For a point scatterer, the actual loss generally lies somewhere between the peak value and no loss. A more reasonable measure of performance is the average straddle loss. Average straddle loss is defined as

$$L_{\text{st\_avg}} = 10\log_{10}\left(\frac{1}{\Delta t}\int_{-\Delta t/2}^{\Delta t/2}\left|\frac{y(t)}{y(0)}\right|^2 dt\right) \tag{20.47}$$

Peak and average straddle losses are a function of the shape of the match filtered response. The sharper the roll-off in amplitude the greater the straddle loss for a given sample spacing.

20.5 PULSE COMPRESSION WAVEFORMS

A simple, unmodulated pulse exhibits a coupling between energy and range resolution. Lengthening the pulse to increase the waveform's transmit energy degrades range resolution, and decreasing the pulse width to achieve finer range resolution reduces the energy. Pulse compression waveforms decouple energy and resolution by exploiting amplitude, phase, or frequency modulation to increase the waveform bandwidth while maintaining the pulse length, with the result that $B \gg 1/\tau$. The application of pulse compression waveforms originated near the end of World War II with the development of the linear frequency modulated waveform [4,12]. Since that time, numerous waveform modulations and processing techniques have been developed and employed. The breadth of modulations reflects the challenge of operating within the constraints of the radar hardware and requirements imposed by targets and interference.

20.5.1 Amplitude Modulation

Intrapulse amplitude modulation could be used to increase a waveform's bandwidth but at a cost of reduced efficiency. Traditionally, intrapulse amplitude modulation has not been employed in radar; however, amplitude modulated waveforms are described in the literature. An example is the Huffman coded waveform [13,14]. Huffman codes employ intrapulse amplitude and phase modulation to tailor the range sidelobes.

20.5.2 Frequency Modulation

In modern systems, both intra- and interpulse frequency modulations are employed. Intrapulse frequency modulated waveforms include both linear and nonlinear modulations [2,4,7]. The LFM waveform is employed in a large number of modern systems and exhibits some unique properties. The LFM waveform has also been combined with *stretch processing* [15] to achieve a reduction in processing bandwidth while preserving the resolution afforded by the transmit bandwidth. Stretch processing is employed in many high-range resolution (HRR) systems including SARs. *Nonlinear frequency modulated* (NLFM) waveforms achieve low-range sidelobes through modulation and circumvent the need to employ an amplitude weighting.

Interpulse modulation is applied in systems where some component of the hardware limits the instantaneous (i.e., intrapulse) bandwidth. A stepped frequency waveform

[16,17] employs interpulse modulation. The waveform consists of a series of narrow band pulses that are transmitted at different frequencies to create a large composite bandwidth. On receive, the pulses are combined coherently to achieve fine range resolution. Stepped frequency waveforms are also known as synthetic wideband waveforms. A stepped chirp [18] is another example of an interpulse modulated waveform. The individual pulses comprising a stepped chirp waveform are linear frequency modulated and separated in frequency. The returns from successive pulses are stitched together in the signal processor to create the return from a wider bandwidth LFM waveform.

20.5.3 Phase-Coded Waveforms

Phase-coded waveforms consists of N concatenated subpulses (or chips) where the phase is intentionally varied subpulse to subpulse to achieve a desired mainlobe and sidelobe response. In general, the length of an individual subpulse defines the range resolution of the waveform. Phase-coded waveforms are grouped into two categories: biphase and polyphase. Biphase-coded waveforms exhibit two possible phase states, typically 0 and 180 degrees, while polyphase codes exhibit more than two phase states. In general, the sidelobe levels of a phase-coded waveform decrease with increasing code length (number of subpulses). Phase-coded waveforms have been identified that yield the minimum peak sidelobe level [19–24] for a given code length. In addition, phase codes have been identified that yield low, predictable sidelobe levels and that are easy to synthesize [2,6,7,25,26]. Phase codes may also be designed address to Doppler tolerance [27] and electromagnetic interference [7,28].

20.6 PULSE COMPRESSION GAIN

Pulse compression gain is defined as the ratio of the SNR at the output of the matched filter to that prior to the filter. In a radar system, an anti-aliasing filter precedes the analog-to-digital converter (ADC). The anti-aliasing filter is generally a linear phase filter with a bandwidth matched to the waveform bandwidth, B. The filter limits the noise bandwidth to that of the waveform and supports Nyquist sampling by rejecting out-of-band signals. The SNR at the output of the anti-aliasing filter is defined by the radar range equation in equation (20.3).

When employing a pulse compression waveform, the matched filter follows the anti-aliasing filter in a digital implementation. The matched filter accounts for the waveform modulation and thus coherently integrates the waveform samples. In contrast, noise samples are noncoherently integrated. The net result is a gain in SNR at the output of the matched filter. The gain is also present with an analog implementation of the matched filter.

Pulse compression gain is defined by the waveform's *time-bandwidth* (TB) *product* τB. The resultant SNR is

$$SNR = \frac{P_t G_t G_r \lambda^2 \sigma}{(4\pi)^3 R^4 k T_s B L_s} \tau B = \frac{P_t \tau G_t G_r \lambda^2 \sigma}{(4\pi)^3 R^4 k T_s L_s} \tag{20.48}$$

and reduces to the energy form of the radar range equation. In many cases, the SNR at the output of the ADC is less than 0 dB. It is only after applying the matched filter that the signal appears above the noise floor. In modern systems, time-bandwidth products can range from 1 (for a simple pulse) to 10^6 or greater.

20.7 | LINEAR FREQUENCY MODULATED WAVEFORMS

During World War II, the need to detect targets at extended ranges and limits on transmit power forced radar engineers to employ long pulses to improve detection at the expense of degraded range resolution. However, near the end of the war, American, British, and German scientists were experimenting with intrapulse modulated waveforms and dispersive filters that, when combined, decoupled waveform energy and resolution. The war ended in 1945, and by the 1950s the once-classified work appeared in patents and papers. The documents describe an LFM waveform and a technique for synthesizing and compressing it [4,12]. The LFM waveform may be described at a high level as a sinusoid whose frequency changes linearly with time. The pulse is compressed by taking advantage of the fact that the propagation delay through a dispersive filter is frequency dependent. The filter time-aligns the frequencies, resulting in a compression of the pulse. The filter may also be used to synthesize the waveform by exciting it with a short CW pulse possessing the desired bandwidth. The frequency-dependent propagation delay through the filter creates an extended length pulse exhibiting a linear time versus frequency relationship.

The LFM waveform has some unique properties and is employed in many modern radar systems supporting search, track, and high-resolution modes. The waveform is considered to be Doppler tolerant and exhibits a range-Doppler coupled ambiguity surface [2,4,6,7]. The waveform also enables stretch processing [15], which reduces the required processing bandwidth in high-resolution systems.

20.7.1 Time-Domain Description of an LFM Waveform

A baseband LFM pulse is defined as

$$x(t) = A\cos\left(\pi\frac{B}{\tau}t^2\right) \quad -\frac{\tau}{2} \le t \le \frac{\tau}{2} \tag{20.49}$$

where A is the waveform amplitude, B is the waveform bandwidth, and τ is the pulse duration. The time-domain response of an LFM pulse is plotted in Figure 20-7.

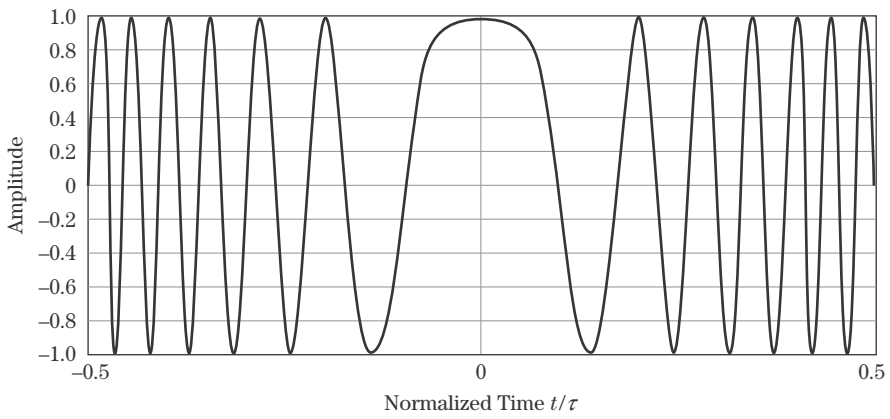

FIGURE 20-7 ■ Time-domain response, within the pulse, of a linear frequency modulated (LFM) waveform with a time-bandwidth product equal to 50.

On transmit, the LFM pulse is centered at an RF f_0 and is expressed as

$$x_{RF}(t) = A\cos\left(2\pi f_0 t + \pi\frac{B}{\tau}t^2\right) \quad -\frac{\tau}{2} \le t \le \frac{\tau}{2} \tag{20.50}$$

In most systems, the RF signal is mixed to baseband prior to compression, and a coherent detector is used in the downconversion process to form in-phase (I) and quadrature (Q) receive channels. The resultant complex, baseband signal is

$$x(t) = A\exp\left(j\pi\frac{B}{\tau}t^2\right) \quad -\frac{\tau}{2} \le t \le \frac{\tau}{2} \tag{20.51}$$

The time-varying phase $\phi(t)$ of an LFM waveform is quadratic

$$\phi(t) = \pi\frac{B}{\tau}t^2 \quad -\frac{\tau}{2} \le t \le \frac{\tau}{2} \tag{20.52}$$

and the instantaneous frequency in radians per second, defined as the derivative of the phase in (20.52), is

$$\frac{d\phi(t)}{dt} = 2\pi\frac{B}{\tau}t \quad -\frac{\tau}{2} \le t \le \frac{\tau}{2} \tag{20.53}$$

The instantaneous frequency in hertz is

$$f(t) = \frac{B}{\tau}t \quad -\frac{\tau}{2} \le t \le \frac{\tau}{2} \tag{20.54}$$

and is plotted in Figure 20-8. Note that the instantaneous frequency is linear with time—thus, the label *linear frequency modulation.* The waveform is commonly referred to as a "chirp" waveform because a similar pulse in the audible frequency range produces a chirping sound.

The plot of instantaneous frequency versus time is often used to depict an LFM waveform. An LFM waveform sweeps through B hertz in τ seconds. The ratio B/τ in (20.54) is the slope of the instantaneous frequency and is termed the *ramp rate* or *sweep rate*.

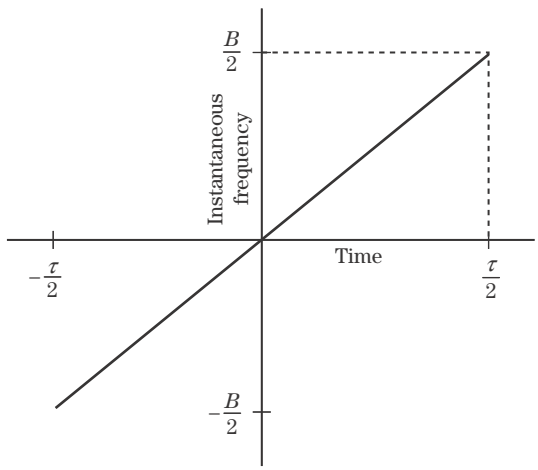

FIGURE 20-8 ■ Instantaneous frequency versus time for an LFM waveform.

20.7.2 Waveform Spectrum

Klauder [12] and Cook [4] provide closed-form expressions for the spectrum of an LFM waveform. The expressions contain Fresnel sine and cosine integrals. However, for reasonable time-bandwidth products (e.g., $\tau B > 10$), the LFM spectrum may be approximated by a much simpler expression

$$X(\omega) \approx |X(\omega)| \exp\left(-j\frac{1}{4\pi}\frac{\tau}{B}\omega^2\right)\exp\left(j\frac{\pi}{4}\right) \tag{20.55}$$

where $|X(\omega)| \approx 1$, $-\pi B \leq \omega \leq \pi B$, and is zero elsewhere. The spectrum in (20.55) consists of rectangle-shaped magnitude response, defined over the swept bandwidth, and a quadratic phase response.

The adequacy of the approximation in equation (20.55) is a function of the waveform TB product. To illustrate the dependence on TB, the spectra associated with two LFM waveforms are presented in Figure 20-9 with time-bandwidth products of 20 (light curve) and 100 (dark curve). As the time-bandwidth product increases, the spectrum becomes more rectangular in shape with a sharper transition region and with a larger percentage of the waveform energy contained within the nominal range of frequencies $-B/2 \leq f \leq B/2$. For $\tau B \geq 100$, approximately 98% to 99% of the waveform energy is contained in this region [12]. Note that neither the peak of the spectral response nor the -3 dB point occurs at $B/2$. For both waveforms, the -6 dB point occurs at approximately $\pm B/2$.

The quadratic phase term in equation (20.55) plays an important role in defining the response in the presence of uncompensated Doppler. The quadratic phase is unique to an LFM waveform and provides it with a degree of Doppler tolerance not found in other waveforms. The contribution of the quadratic phase is examined in Section 20.10.4.

20.7.3 Compressed Response

The compressed response is computed in the time domain by convolving the LFM waveform with its matched filter or

$$y(t) = \frac{1}{\tau}\int \exp\left(j\pi\frac{B}{\tau}\alpha^2\right)\exp\left(-j\pi\frac{B}{\tau}(\alpha - t)^2\right)d\alpha, \quad -\tau \leq t \leq \tau \tag{20.56}$$

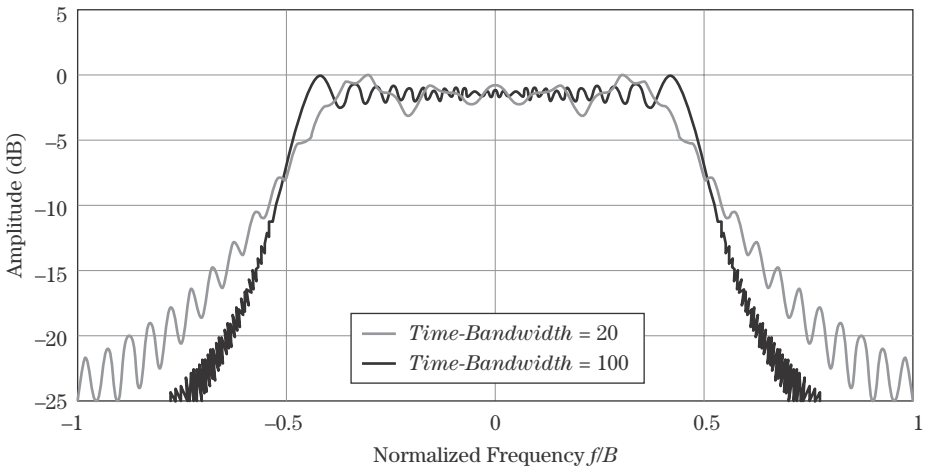

FIGURE 20-9 ■ Comparison of the spectra of LFM waveforms with time-bandwidth products of 20 (light curve) and 100 (dark curve).

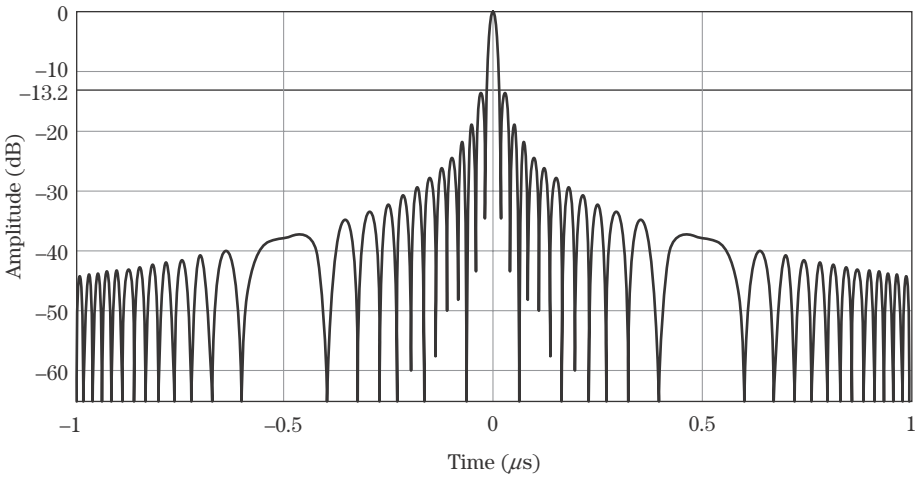

FIGURE 20-10 ■ Match filtered response for a 50 MHz, 1 μsec LFM waveform.

where α is a dummy variable of integration. The waveform and matched filter are both normalized to unity energy. The compressed response obtained by evaluating (2.56) is

$$y(t) = \left(1 - \frac{|t|}{\tau}\right) \frac{\sin\left[\left(1 - \frac{|t|}{\tau}\right)\pi Bt\right]}{\left(1 - \frac{|t|}{\tau}\right)\pi Bt}, \quad |t| \leq \tau \tag{20.57}$$

The response in (20.57) consists of the product of a term resembling a sinc function and a triangle function defined over the time interval $-\tau \leq t \leq \tau$ and zero elsewhere. Figure 20-10 contains a plot of the compressed response for an LFM waveform with a 50 MHz bandwidth and a 1 μsec pulse width ($\tau B = 50$). The peak sidelobes are close to the nominal -13.2 dB peak sidelobes associated with a sinc function.

The argument of the sine function in equation (20.57) may be written as

$$\left(1 - \frac{|t|}{\tau}\right)\pi Bt = \pi Bt - \frac{\pi Bt^2}{\tau}, \quad t \geq 0 \tag{20.58}$$

revealing both a linear and quadratic term. For $t \ll \tau$, the linear term dominates, and the argument is approximately equal to πBt. Thus, in the vicinity of the peak, the response approaches a true sinc function weighted by a triangle. Cook [4] states that for TB products greater than 20 the match filtered response resembles a sinc.

20.7.4 Rayleigh Resolution

Rayleigh resolution is defined as the separation between the peak and the first null of the match filtered response. The first null in (20.57) occurs when the argument of the sine function equals π. For TB products great than 10, the null occurs at

$$t \approx \pm\frac{1}{B} \tag{20.59}$$

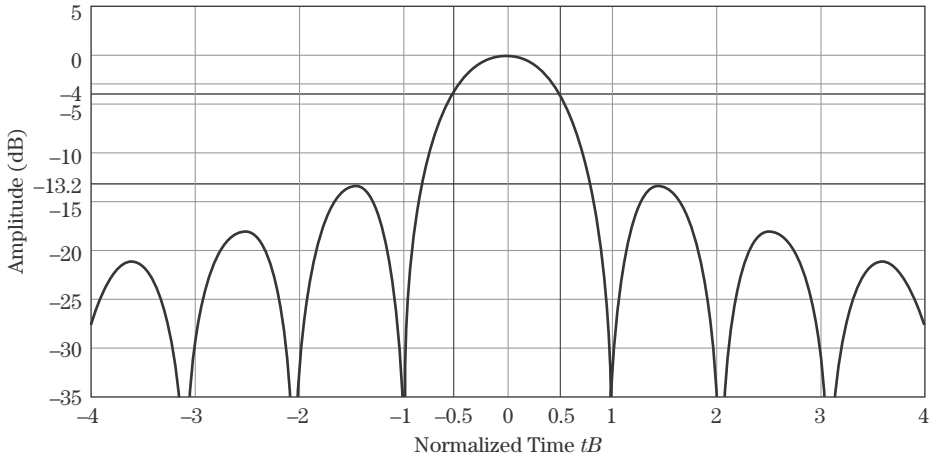

FIGURE 20-11 ■ Mainlobe and first 3 sidelobes for the LFM waveform match filtered response with a time-bandwidth product equal to 100.

Accounting for two-way propagation and the speed of light, the Rayleigh range resolution is

$$\delta R = \frac{c}{2B} \tag{20.60}$$

A portion of the compressed response associated with an LFM with $\tau B = 100$ is provided in Figure 20-11. The Rayleigh time resolution of $1/B$ is also the -4 dB width (provided no amplitude weighting is employed to suppress the range sidelobes). Note that the -3 dB width of the response, also shown in the figure, is less than the -4 dB width or Rayleigh resolution and thus represents a closer spacing between "resolved" scatterers.

20.7.5 The Nominal Sidelobe Response

Pulse compression waveforms exhibit range sidelobes that extend over a time interval equal to twice the pulse width and that are a function of the modulation employed. Sidelobes degrade radar performance by placing energy up and down range from its source. For example, range sidelobes associated with a large RCS target may mask the presence of a smaller target located within a pulse width of the larger target; thus, "low" sidelobes are a desirable property. Sidelobe performance is quantified in terms of both peak and integrated ratios. The *peak sidelobe ratio* (PSR) is defined as the ratio of the peak sidelobe to the peak of the mainlobe.

For time-bandwidth products greater than 20, the peak sidelobes of an LFM waveform are approximately -13.2 dB and occur adjacent to the mainlobe [4]. In general, frequency modulated waveforms exhibit high sidelobes adjacent to or near the mainlobe, and the sidelobes decrease with distance from the mainlobe. For an LFM waveform, the peaks of the sidelobes roll-off as $-20\log_{10}(\pi Bt)$. The minimum sidelobe peak is approximately $-20\log_{10}(\pi B\tau)$. This is illustrated in Figure 20-10 where the minimum sidelobe peak is approximately -44 dB for a time-bandwidth product of 50.

In a distributed clutter or multiple target/scatterer environment, the integrated sidelobe ratio is an important metric. For example, an HRR profile of a vehicle contains returns from scatterers located on the vehicle and returns from neighboring terrain projected onto the vehicle through the range sidelobes. Patches of resolved terrain contribute sidelobe energy onto the vehicle's range profile. The sidelobe energy, originating from resolved

patches distributed in range, adds noncoherently at ranges associated with the vehicle. The cumulative, noncoherent contribution may be sufficient to degrade the HRR profile.

The integrated sidelobe ratio is defined as the ratio of the energy in the sidelobes to the energy in the mainlobe. Integrated sidelobes are a source of multiplicative noise [10] and must be weighted by the average power in the range cells containing the interference to determine their impact. The integrated sidelobe ratio for an unweighted LFM waveform is approximately −9.6 dB [29]. Amplitude weighting lowers the peak sidelobe and reduces the integrated sidelobe ratio (ISR; see Section 20.9).

20.8 MATCHED FILTER IMPLEMENTATIONS

The matched filter or compression operation may be implemented in analog hardware or performed digitally. In most modern systems, compression is performed digitally, but analog implementations still exist. The digital approach overcomes some of the disadvantages associated with analog compression including insertion loss, device dependence on waveform parameters, and pulse width and bandwidth limitations [30]. In addition, digital compression offers advantages including selectable sidelobe control and error compensation. A brief discussion of analog approaches is presented, followed by a more in-depth discussion of digital compression.

20.8.1 Dispersive Filters

Dispersive analog filters may be used to synthesize and compress an LFM pulse. Dispersive filters exhibit a time delay through the filter that is a function of frequency. A filter's dispersion is characterized by its *group delay*, t_{gd}, which is defined as the negative of the derivative of the filter's frequency-domain phase response $\Phi(\omega)$ or

$$t_{gd} = -\frac{d\Phi(\omega)}{d\omega} \tag{20.61}$$

The LFM waveform's phase response in (20.55) yields a group delay of

$$t_{gd\_LFM} = \frac{\tau}{2\pi B}\omega \tag{20.62}$$

The matched filter's group delay is

$$t_{gd\_LFM\_MF} = -\frac{\tau}{2\pi B}\omega \tag{20.63}$$

given the conjugate relationship between the waveform and matched filter spectrum.

A dispersive filter may be used to both expand and compress a pulse. A CW pulse with duration $1/B$ passing through a dispersive filter with group delay defined in (20.62) experiences a time expansion, producing a pulse of duration τ. The expansion occurs as each frequency component of the signal is delayed by a variable amount of time. The result is a linear frequency modulated pulse.

The pulse is compressed using a filter with the opposite sense phase, or negative group delay. The frequency-dependent delay aligns the various frequency components in time. The filter coherently integrates the response, producing a compressed pulse.

Bulk acoustic wave (BAW) and surface acoustic wave (SAW) devices are dispersive filters used in some radar systems. Farnett and Stevens [30] describe the performance of BAW and SAW devices. These devices exhibit *insertion loss* and are limited in the pulse lengths and bandwidths they support.

20.8.2 Digital Filters

Modern radars may employ either voltage-controlled oscillators or digital waveform generators to precisely modulate the transmit waveform. On receive, digital compressors have replaced their analog counterparts. A digital compressor correlates the digitized signal with a stored copy of the matched filter. The correlation operation may be implemented using fast Fourier transforms (FFTs) by exploiting the duality between correlation in the time-domain and multiplication in the frequency domain [31]. FFTs are efficient implementations of the discrete Fourier transform (DFT), which transforms discrete time samples into samples of the discrete-time Fourier transform (DTFT; see Chapter 14). The correlation operation, implemented using FFTs, is commonly referred to as *fast convolution* [32].

An illustration of a coherent receiver followed by a digital compressor is shown in Figure 20-12. In general, the received RF signal is mixed to some IF prior to mixing the signal to baseband. The analog signal at IF is denoted as $x_{IF}(t)$ in the figure. The IF signal is fed into a quadrature detector where in-phase $x_I(t)$ and quadrature phase $x_Q(t)$ signals are generated. The analog in-phase and quadrature signals are then fed into separate ADCs. The Nyquist sampling theorem requires that each signal (or channel) be sampled at a rate equal to or greater than twice the highest frequency component. For a baseband-centered, band-limited signal, the highest frequency is equal to one-half the bandwidth. The ADC is therefore required to sample at a rate equal to or greater than the waveform bandwidth. The baseband filter is designed with a bandwidth equal to the waveform bandwidth and suppresses out-of-band signals that alias. The in-phase and quadrature signals may be interpreted as the real and imaginary parts, respectively, of a complex signal. The digitized, complex signal is

$$x[n] = x_I[n] + jx_Q[n] \tag{20.64}$$

In some modern systems, sampling is performed at IF and the in-phase and quadrature channels are created digitally. In this case, the required sampling rate is greater than twice the waveform bandwidth (2.5 to 4 times the bandwidth depending on the implementation), and controlled aliasing is used to create a real, sampled signal centered at a frequency

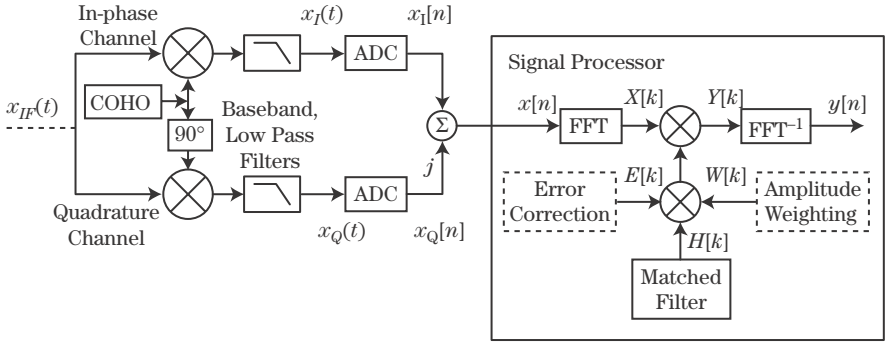

FIGURE 20-12 ■ Fast convolution is one way to implement digital pulse compression.

offset from baseband [6]. IF sampling circumvents the requirement to balance the analog in-phase and quadrature channels in both amplitude and phase.

In general, radar systems are designed to collect returns over a specified *range window*. A range window is defined in terms of a start range and an end range. The receiver is activated at a time delay corresponding to the start range and deactivated at a time delay corresponding to the completion of the collection interval that includes the end range. The time delay or extent associated with a range window is

$$T_{R_w} = \frac{2R_w}{c} \tag{20.65}$$

where R_w is the range extent of the window. To prevent eclipsing, a full pulse is collected from the beginning and end of the range window. The minimum collection time is therefore

$$T_C = \tau + \frac{2R_w}{c} \tag{20.66}$$

The number of complex samples collected over a range window is equal to the product of the ADC sampling rate and the collection time, or

$$N_{RW} = F_s\left(\tau + \frac{2R_w}{c}\right) \tag{20.67}$$

The digital compressor, employing fast convolution, receives the digitized signal $x[n]$ and passes it through the first FFT (or DFT), as shown in Figure 20-12. The DFT yields

$$x[n] \overset{DFT}{\longleftrightarrow} X[k] \tag{20.68}$$

where $X[k]$ is the DFT spectrum of the received signal. The matched filter's spectrum is defined by $H[k]$ and is generally precomputed and stored in memory. The compressor forms the product

$$Y[k] = X[k]H[k] \tag{20.69}$$

and the inverse transform yields

$$Y[k] \overset{DFT^{-1}}{\longleftrightarrow} y[n] \tag{20.70}$$

where $y[n]$ is the output of the filter. To ensure linear convolution over the entire range window, it is necessary to use the collection time in equation (20.66) as well as an appropriate DFT size (see Chapter 14).

As a waveform passes through the transmitter and receiver, modulations are induced that create a mismatch between the ideal matched filter and the received waveform. Extraneous modulations may cause an increase in the range sidelobes, a degradation in resolution, and a loss in processing gain. An error correction filter may be used to compensate for repeatable modulation errors. The error correction filter is formed using a *pilot pulse*. A pilot pulse consists of a copy of the transmit waveform that is propagated through the transmit/receive chain and, if radiated externally, may be reflected from a preselected point source (e.g., a corner reflector). The pilot pulse is modulated by error sources and is digitized on receive. The digitized signal is used to form an error compensation filter $E[k]$, as depicted in Figure 20-12. The error filter takes the place of an ideal matched filter. In general, phase modulations are the easiest to compensate for and are removed by applying the conjugate phase. When compensating for amplitude modulation, care must be taken to avoid division by zero.

20.9 | SIDELOBE REDUCTION IN AN LFM WAVEFORM

An LFM waveform's peak sidelobe ratio is −13.2 dB. The high peak sidelobes are a result of the spectrum's sharp transition regions, as illustrated in Figure 20-9. To reduce the nominal sidelobes, an amplitude weighting may be applied to the spectrum. The weighting tapers the spectrum's band edges or transition regions and produces a reduction in the peak sidelobe level. Amplitude weighting represents an intentional mismatch between the filter and the transmit waveform, which lowers the sidelobes but at a cost of degraded resolution and loss in processing gain.

A *Taylor weighting* is often applied in radar and achieves the minimum mainlobe width for a given peak sidelobe level conditioned on the fact that sidelobes decrease with distance from the mainlobe. The Taylor weighting is defined by two parameters: the peak sidelobe ratio, *PSR*, and the total number of sidelobes, $\overline{n}$, adjacent to the mainlobe beyond which the sidelobes start to decrease.

The Taylor weighting function, $W_{Taylor}(\omega)$, is defined by [2,4]

$$W_{Taylor}(\omega) = K\left\{1 + 2\sum_{m=1}^{\bar{n}-1} F_m \cos\left(\frac{m\omega}{B}\right)\right\} \quad -\pi B \le \omega \le \pi B \tag{20.71}$$

where

$$F_m = \begin{cases} \dfrac{(-1)^{m+1}\prod_{n=1}^{\bar{n}-1}\left[1 - \dfrac{m^2}{S(D^2 + (n-0.5)^2)}\right]}{2\prod_{\substack{n=1 \\ n\neq m}}^{\bar{n}-1}\left(1 - \dfrac{m^2}{n^2}\right)}, & m = 1, 2, \ldots, (\bar{n}-1) \\ 0, & m \ge \bar{n} \end{cases} \tag{20.72}$$

$$D = \frac{1}{\pi}\cosh^{-1}\left[10^{-PSR/20}\right] \tag{20.73}$$

$$S = \frac{\bar{n}^2}{D^2 + (\bar{n} - 0.5)^2} \tag{20.74}$$

and

$$K = \frac{1}{1 + 2\sum_{m=1}^{\bar{n}-1} F_m} \tag{20.75}$$

In equation (20.71), the spectral extent of the Taylor weighting is matched to the LFM waveform's bandwidth. The continuous weighting function in (20.71) is sampled at the DFT frequency bin spacing to produce a discrete weighting function, or

$$W_{Taylor}[k] = K\left\{1 + 2\sum_{m=1}^{\bar{n}-1} F_m \cos\left(\frac{m2\pi k}{M}\right)\right\}, \quad k = \left(-\frac{M}{2} + 1\right), \ldots, 0, \ldots, \frac{M}{2} \tag{20.76}$$

where M is the DFT size and is assumed to be even in this case. Nyquist sampling is assumed with $F_s = B$.

TABLE 20-1 ■ SNR Loss Associated with a Taylor Weighting Function

	Peak Sidelobe Ratio (dB)								
	−20	−25	−30	−35	−40	−45	−50	−55	−60
$\overline{n}$	SNR Loss (dB)								
2	−0.21	−0.38	−0.51						
3	−0.21	−0.45	−0.67	−0.85					
4	−0.18	−0.43	−0.69	−0.91	−1.11	−1.27			
5	−0.16	−0.41	−0.68	−0.93	−1.14	−1.33	−1.49		
6	−0.15	−0.39	−0.66	−0.92	−1.15	−1.35	−1.53	−1.68	
7	−0.15	−0.37	−0.65	−0.91	−1.15	−1.36	−1.54	−1.71	−1.85
8	−0.16	−0.36	−0.63	−0.90	−1.14	−1.36	−1.55	−1.72	−1.87

The loss in SNR due to weighting is [6]

$$SNR_{loss} = \frac{\left[\sum_{k=-M/2+1}^{M/2} W[k]\right]^2}{M \sum_{k=-M/2+1}^{M/2} W^2[k]} \tag{20.77}$$

where $W[k]$ are the weighting coefficients indexed by k, and M is the number of coefficients. Table 20-1 contains processing losses for a Taylor window as a function of PSR and $\overline{n}$. Note that the loss increases with decreasing sidelobe level.

Weighting inherently reduces the waveform bandwidth resulting in degraded resolution. For a Taylor weighting, the mainlobe width, measured at the −4 dB point, is recorded in Table 20-2 for different values of PSR and $\overline{n}$. The −4 dB point was chosen since it corresponds to the Rayleigh resolution associated with an unweighted LFM waveform. The resolutions reported in Table 20-2 are normalized by $c/2B$ (i.e., the nominal Rayleigh resolution).

Figure 20-13 contains a portion of the response associated with an LFM waveform with (solid curve) and without (dashed curve) weighting. For the weighted case, a −40 dB, $\overline{n} = 4$, Taylor weighting has been applied. The waveform's time-bandwidth product is 500. The reduced sidelobes and mainlobe broadening are apparent. The peak sidelobe ratio is approximately −38 dB (2 dB above the design level of −40 dB). The elevated

TABLE 20-2 ■ 4 dB Resolution Associated with a Taylor Weighting Function

	Peak Sidelobe Ratio (dB)								
	−20	−25	−30	−35	−40	−45	−50	−55	−60
$\overline{n}$	4 dB Resolution Normalized by $c/2B$								
2	1.15	1.19	1.21						
3	1.14	1.22	1.28	1.33					
4	1.12	1.22	1.29	1.36	1.42	1.46			
5	1.11	1.20	1.29	1.36	1.43	1.49	1.54		
6	1.10	1.19	1.28	1.36	1.43	1.50	1.56	1.61	
7	1.09	1.19	1.28	1.36	1.43	1.50	1.56	1.62	1.67
8	1.08	1.18	1.27	1.35	1.43	1.50	1.57	1.63	1.68

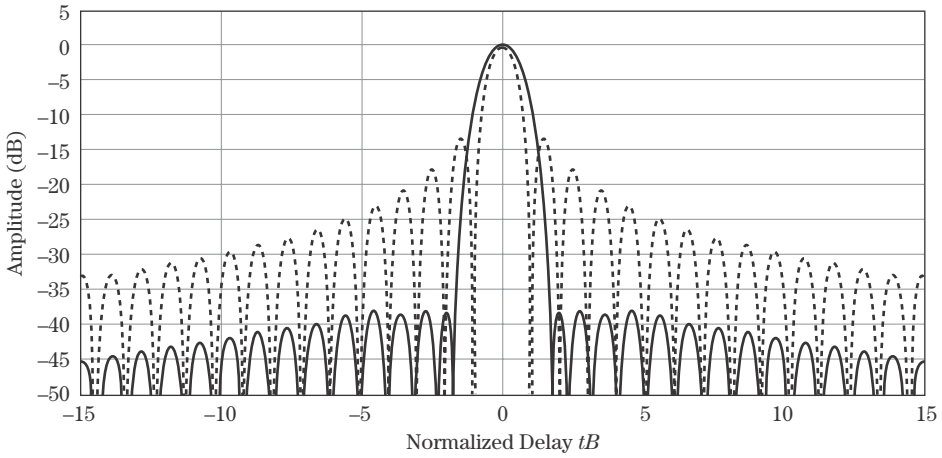

FIGURE 20-13 ■ A -40 dB, $\overline{n} = 4$, Taylor-weighted LFM waveform compressed response (solid curve) has significantly reduced sidelobes versus an unweighted LFM waveform response (dashed curve).

sidelobes are explained in the next section. Both responses have been normalized to their respective peak values so the loss in energy due to weighting is not apparent. Note that when applying a weighting it is the loss in SNR and not the loss in the waveform's energy that dictates performance.

20.9.1 Weighting and Time-Bandwidth Requirements

For a given taper, the expected sidelobe performance is achieved by applying the weighting to a signal with a rectangular envelope. The LFM waveform's spectrum is not a perfect rectangle, and therefore, some degradation in sidelobe performance is expected. As discussed in Section 20.7.2, the transition region sharpens with increasing time-bandwidth product, producing a more compact spectrum. As a result, sidelobes approach the design level as the time-bandwidth product is increased. Cook [4] states that a time-bandwidth product greater than 100 is required to achieve a peak sidelobe close to the taper's expected level.

A comparison of compressed responses for TB products of 20 and 100 is shown in Figure 20-14. A -40 dB, $\overline{n} = 4$, Taylor weighting is applied. The peak sidelobe associated with $\tau B = 20$ is -23.3 dB, and the peak sidelobe associated with $\tau B = 100$ is -35 dB.

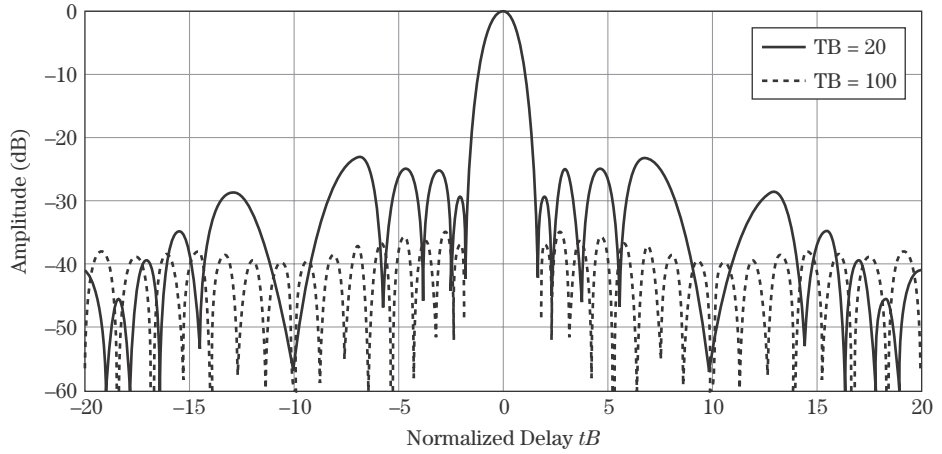

FIGURE 20-14 ■ A comparison of time-sidelobe responses for time-bandwidth products of 20 (solid curve) and 100 (dashed curve) when applying a -40 dB Taylor weighting.

TABLE 20-3 ■ Peak and Average Straddle Loss Associated with a Taylor Weighted LFM with $\tau B = 500$

	Peak Sidelobe Ratio (dB)									
	−20		−30		−40		−50		No Weighting	
	Straddle Loss									
$\bar{n}$	Peak	Average	Peak	Average	Peak	Average	Peak	Average	Peak	Average
3	−2.99	−0.89	−2.35	−0.72	−2.02	−0.63	−1.83	−0.57		
4	−3.07	−0.91	−2.32	−0.71	−1.93	−0.60	−1.69	−0.53		
5	−3.15	−0.93	−2.33	−0.71	−1.90	−0.59	−1.63	−0.51		
6	−3.21	−0.94	−2.35	−0.72	−1.89	−0.59	−1.61	−0.51	−3.92	−1.12
7	−3.25	−0.96	−2.37	−0.72	−1.89	−0.59	−1.59	−0.50		
8	−3.28	−0.96	−2.38	−0.73	−1.90	−0.59	−1.59	−0.50		

Note: The sampling rate is equal to the nominal waveform bandwidth, B.

Time sidelobes are shown to approach the design level as the time-bandwidth product is increased. For the case of a low time-bandwidth product, a heavier weighting may be applied to further reduce the sidelobes at the cost of additional SNR loss and degraded range resolution.

Phase codes, to be discussed in Section 20.12, are often used in lieu of frequency modulated pulses when low time-bandwidth products are driven by system constraints. For example, a 13-bit biphase Barker code achieves a −22.3 dB peak sidelobe with a time-bandwidth product of 13 and with no amplitude taper applied.

20.9.2 Straddle Loss Reduction

In addition to lowering the sidelobes, an amplitude taper reduces straddle loss. As discussed in Section 20.4, straddle loss is the loss in SNR that occurs when the peak of the match filtered response is not sampled. In most systems, the ADC sampling rate is proportional to the receive waveform bandwidth. For a fixed sampling rate, a broadening of the mainlobe reduces the straddle loss by decreasing the slope of the response near the peak and, as a result, diminishes the amplitude difference between the peak and the nearest sample. Table 20-3 contains peak and average straddle losses for a Taylor weighted LFM with a time-bandwidth product of 500. The waveform is sampled at a rate equal to the waveform bandwidth prior to weighting. Included in the table is the straddle loss associated with no weighting. Without weighting, the peak straddle loss is approximately −4 dB, and the average loss is about −1 dB. For a 40 dB Taylor, the peak straddle loss is approximately −1.9 dB, and the average loss is about −0.6 dB. This represents a reduction (improvement) in peak straddle loss of approximately 2 dB and a reduction in average loss of 0.4 dB.

20.10 AMBIGUITY FUNCTIONS

The matched filter defined in equation (20.31) is predicated on the assumption that the received waveform is an amplitude-scaled and time-delayed version of the transmit waveform. When a radial velocity component exists between the radar and a target, a Doppler shift is imparted to the waveform. A Doppler shift [33] is defined as a shift in frequency

due to relative motion. The shift is computed as

$$f_d = \frac{2v_r}{\lambda} \tag{20.78}$$

where v_r is the radial component of velocity. For closing (approaching) targets, the sign of the radial velocity is positive so that the Doppler shift is positive, representing an increase in frequency. For opening targets, the sign of the radial velocity is negative and the Doppler shift is negative, indicating a decrease in frequency.

Without a priori knowledge, the Doppler shift represents an unintentional mismatch between the received waveform and the matched filter. In some cases, the Doppler shift is estimated and removed prior to applying the matched filter. However, some residual or uncompensated Doppler typically remains.

Ambiguity functions are used to characterize the response of the matched filter in the presence of uncompensated Doppler. The ambiguity function is defined as

$$A(t,\, f_d) = \left| \int x(\alpha) \exp\left(j2\pi f_d \alpha\right) x^*\left(\alpha - t\right) d\alpha \right| \tag{20.79}$$

where $x(\alpha)\exp(j2\pi f_d\alpha)$ is the Doppler-shifted waveform, and α is a dummy variable of integration. For $f_d = 0$, the ambiguity response is simply the magnitude of the match filtered response.

A three-dimensional plot of the ambiguity function is termed an *ambiguity surface*. To facilitate comparison of ambiguity surfaces, the waveform and matched filter are normalized to unit energy. A unit energy $x_u(t)$ instantiation of the waveform $x(t)$ is obtained via the normalization

$$x_u(t) = \frac{x(t)}{\sqrt{\int |x(t)|^2 dt}} \tag{20.80}$$

Several properties associated with an ambiguity function or surface are worthy of note. An ambiguity surface achieves its maximum value at zero delay and zero Doppler, or at $A(0, 0)$, and, if the waveform is normalized to unit energy, $A(0, 0) = 1$. The volume under the square of the ambiguity surface is unity

$$\int_{-\infty}^{\infty} \int_{-\infty}^{\infty} |A(t,\, f_d)|^2 dt\, df_d = 1 \tag{20.81}$$

given a unit energy waveform. The relationship in (20.81) implies that a waveform designed to lower the response in a given region of the ambiguity surface will produce an increase in another region because the total volume must remain constant. Additional information on ambiguity surfaces is provided in [4,7,34].

In designing a waveform to support a given mode of operation, a number of factors including energy, resolution, blind range extent, duty cycle, and Doppler tolerance must be considered. *Doppler tolerance* refers to the response of a waveform in the presence of uncompensated Doppler and may be assessed using an ambiguity surface.

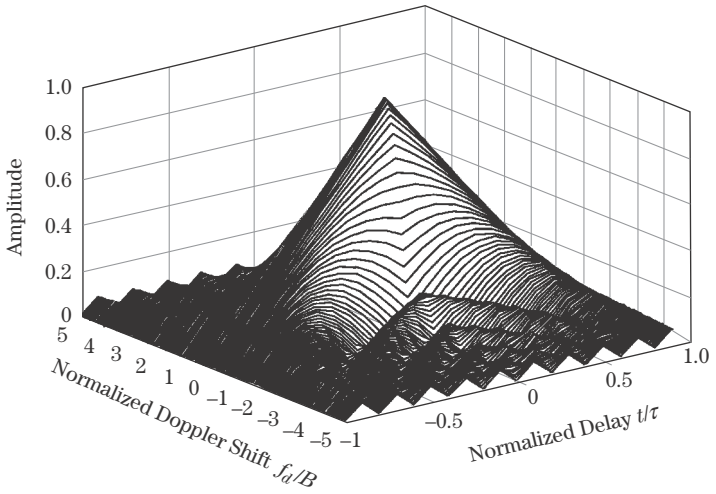

FIGURE 20-15 ■ The ambiguity surface for a simple pulse.

20.10.1 Ambiguity Function for a Simple Pulse

The ambiguity surface for a simple pulse is examined to contrast it with the surface associated with an LFM waveform. For an unmodulated pulse

$$x(t) = \frac{1}{\sqrt{\tau}} \qquad -\frac{\tau}{2} \le t \le \frac{\tau}{2} \tag{20.82}$$

with unit energy and pulse width τ, the ambiguity function [8] is

$$A(t,\, f_d) = \left| \left(1 - \frac{|t|}{\tau}\right) \frac{\sin\left(\pi f_d \tau \left(1 - \dfrac{|t|}{\tau}\right)\right)}{\pi f_d \tau \left(1 - \dfrac{|t|}{\tau}\right)} \right| \qquad |t| \le \tau \tag{20.83}$$

The ambiguity function in (20.83) is plotted in Figure 20-15 and is termed a *ridged* ambiguity surface [8,34]. In the figure, the time-delay axis is normalized by the pulse width, and the Doppler axis is normalized by the waveform bandwidth.

The surface exhibits a peak value at $A(0, 0)$. For $f_d = 0$ the ambiguity function reduces to the magnitude of the match filtered response for a simple pulse, or

$$A(t, 0) = \left| 1 - \frac{|t|}{\tau} \right| \qquad |t| \le \tau \tag{20.84}$$

A cut through the ambiguity surface at zero time delay characterizes the decrease in the peak value as a function of Doppler shift. The zero delay cut is a sinc function

$$A(0,\, f_d) = \left| \frac{\sin(\pi f_d \tau)}{\pi f_d \tau} \right| \qquad |t| \le \tau \tag{20.85}$$

The response is maximum at zero Doppler and is zero at multiples of $1/\tau$. A Doppler shift equal to $1/\tau$ represents a full cycle of Doppler across the pulse and annihilates the peak at zero delay. With one-quarter cycle of Doppler, the peak value is reduced by 1 dB.

20.10.2 Ambiguity Function for an LFM Waveform

A closed-form expression of the LFM waveform's ambiguity surface exists. For a unit energy LFM waveform

$$x(t) = \frac{1}{\sqrt{\tau}} \exp\left(j\pi \frac{B}{\tau} t^2\right) \quad |t| \leq \frac{\tau}{2} \tag{20.86}$$

the ambiguity function is [2,4,6–8]

$$A(t, f_d) = \left| \left(\left(1 - \frac{|t|}{\tau}\right) \frac{\sin\left[\pi\tau\left(1 - \frac{|t|}{\tau}\right)\left(f_d + \frac{B}{\tau}t\right)\right]}{\pi\tau\left(1 - \frac{|t|}{\tau}\right)\left(f_d + \frac{B}{\tau}t\right)} \right) \right| \quad |t| \leq \tau \tag{20.87}$$

As expected, a cut through the ambiguity response along the time-delay axis at zero Doppler is simply the magnitude of the match filtered response in equation (20.57), or

$$A(t, 0) = \left| \left(1 - \frac{|t|}{\tau}\right) \frac{\sin\left[\left(1 - \frac{|t|}{\tau}\right)\pi B t\right]}{\left(1 - \frac{|t|}{\tau}\right)\pi B t} \right| \quad |t| \leq \tau \tag{20.88}$$

20.10.3 Range-Doppler Coupling

An LFM waveform exhibits a coupling between range and Doppler. A Doppler shift translates the peak of the response along the time delay axis by an amount equal to $-(f_d/B)\tau$. The translation can be readily seen by comparing the arguments of the sine functions in equation (20.87) and equation (20.88). Note that the triangle $(1 - t/|\tau|)$ is not shifted and serves to reduce the amplitude of the time-shifted response. Figure 20-16 contains a plot of the ambiguity surface for an LFM waveform with a time-bandwidth

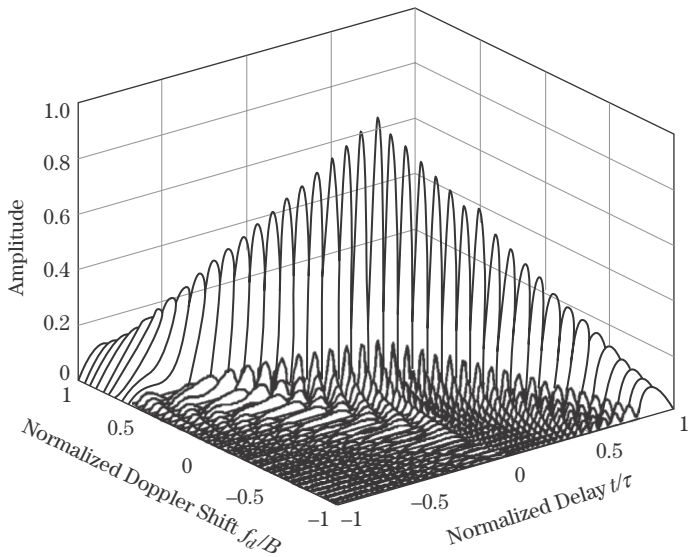

FIGURE 20-16 ■ The ambiguity surface for an LFM waveform with $\tau B = 20$.

product of 20. The surface is coarsely sampled in Doppler to aid the reader in visualizing the affects of range-Doppler coupling.

The LFM waveform exhibits a diagonal ridge in the (t, f_d) plane. For a Doppler shift equal to the inverse of the pulse width (equivalently, one cycle of Doppler across the uncompressed pulse), the peak of the response is shifted by a time delay equal to the Rayleigh resolution of an unweighted LFM waveform, and the peak is reduced by $(1 - 1/B\tau)$ (in voltage). In contrast, a single cycle of Doppler across a simple pulse drives the peak of the response to zero without the reemergence of a discernable mainlobe located at another time delay. The ambiguity surface for an LFM waveform is termed a *sheared ridge*.

The ratio of Doppler shift to waveform bandwidth is termed the *fractional Doppler shift* (FDS). An LFM waveform is considered *Doppler tolerant* given the preservation of the mainlobe and sidelobe structure in the presence of large fractional Doppler shifts (up to 50% or more).

Figures 20-17, 20-18, and 20-19 contain plots of the shift in the peak location, the loss in peak amplitude, and the degradation in resolution, respectively, for time-bandwidth products of 10, 100, and 1,000. The degradation in each metric is gradual and approximately linear for fractional Doppler shifts up to 50%.

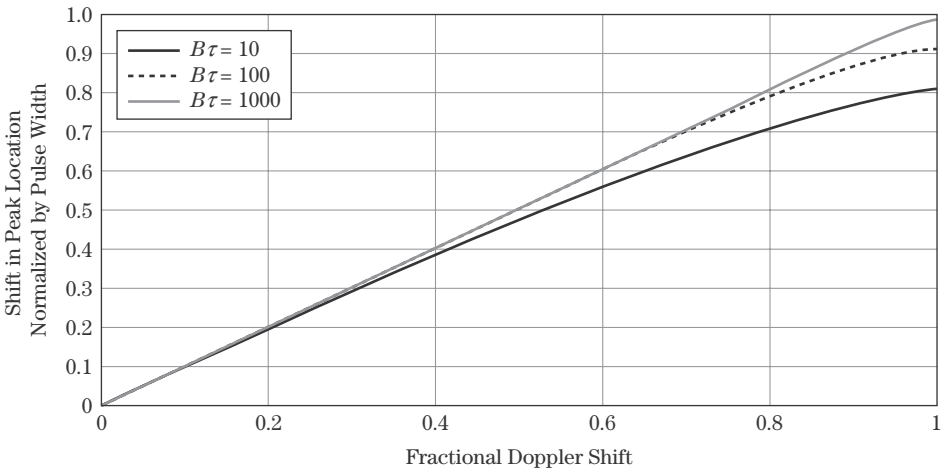

FIGURE 20-17 ■ Time shift in the peak of an LFM waveform's match filtered response as a function of Doppler shift.

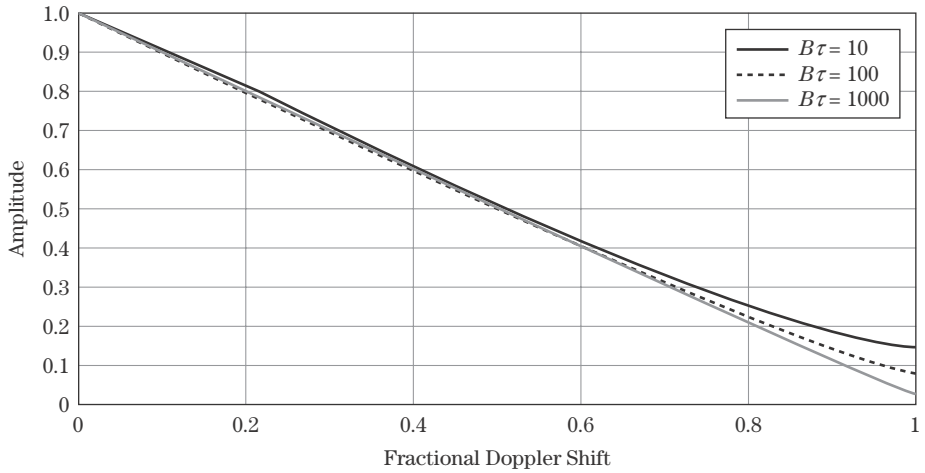

FIGURE 20-18 ■ Reduction in peak amplitude as a function of Doppler shift.

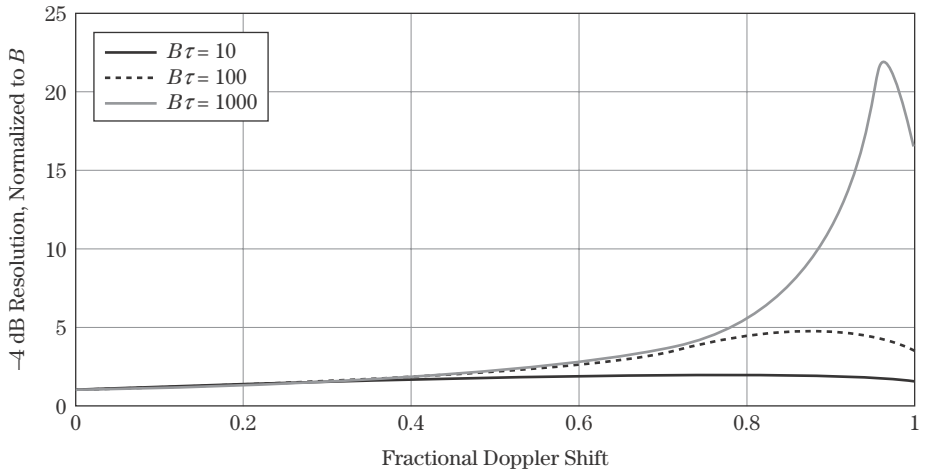

FIGURE 20-19 ■ Increase in −4 dB mainlobe width as a function of Doppler shift.

The sidelobe structure of the LFM waveform is also preserved in the presence of large fractional Doppler shifts. Figure 20-20 contains the compressed range response for an LFM waveform with a time-bandwidth product of 100 at fractional Doppler shifts of 0%, 25%, 50%, and 75%. The sidelobe structure is well behaved, and the peak sidelobe remains 12 to 13 dB below the peak of the mainlobe.

The sidelobe structure in the presence of uncompensated Doppler is not as well behaved when amplitude weighting is applied. The misalignment of the received waveform and the matched filter spectra, combined with amplitude weighting, produces a nonsymmetric weighting that degrades the sidelobe response. Figure 20-21 contains a plot of the compressed response for a −40 dB Taylor-weighted LFM waveform having a time-bandwidth product of 200. The fractional Doppler shifts are 0% (solid curve) and 15% (dotted curve), and the individual curves have been normalized to the peak of their responses. The response with no Doppler shift exhibits peak sidelobes of −38 dB, whereas the response experiencing a 15% fractional Doppler shift exhibits peak sidelobes of −25 dB, well short of the intended −40 dB.

The impact of Doppler should be considered when applying a weighting function to reduce the sidelobes. In general, the heavier the weighting the more the sidelobes degrade as a function uncompensated Doppler. Low sidelobes are often associated with tracking,

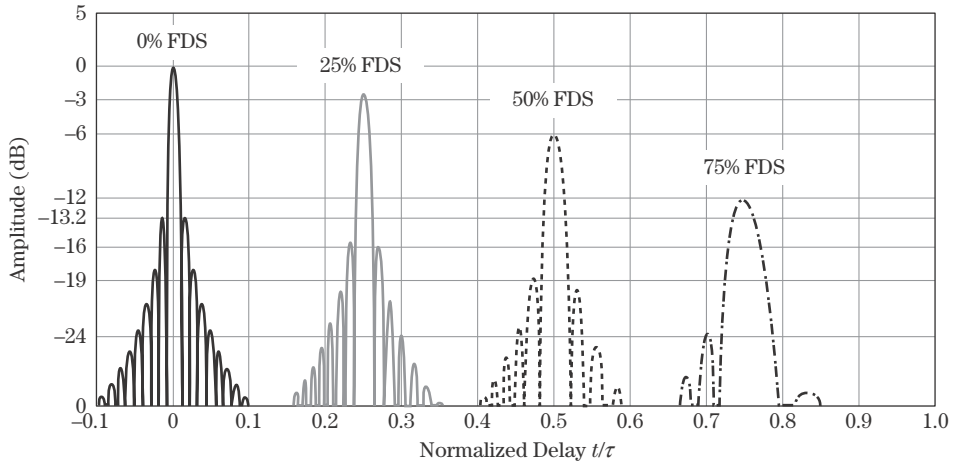

FIGURE 20-20 ■ Individual LFM match filtered responses for fractional Doppler shifts of 0%, 25%, 50%, and 75% illustrate both reduction in peak levels and broadening of the mainlobe.

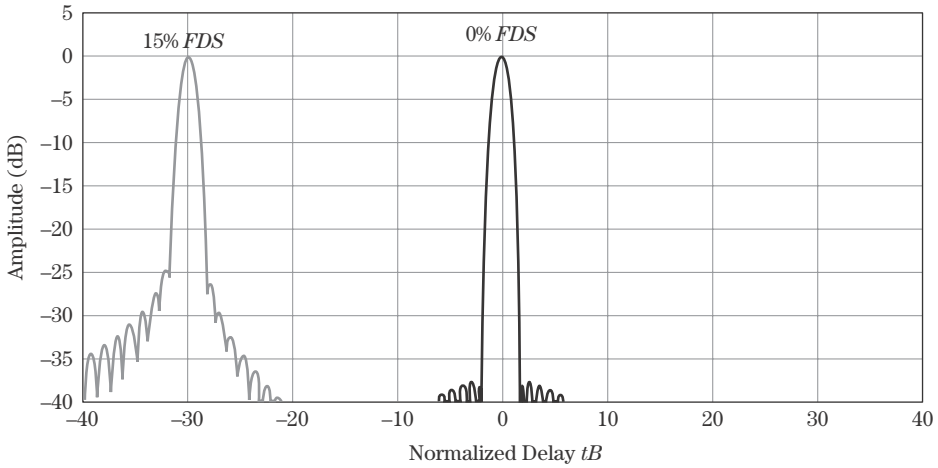

FIGURE 20-21 ■ Match filtered response for a −40 dB Taylor weighted LFM waveform with a time-bandwidth product of 200 and a fractional Doppler shift of 0% (dark curve) and 15% (light curve). Both curves have been normalized to the peak of their responses.

imaging, and discrimination. These radar modes may be supported by Doppler estimation techniques, which compensate for Doppler and thus reduce the impact on the compressed response.

In these examples, a large fractional Doppler shift has been used to illustrate the Doppler tolerance of an LFM waveform; however, fractional Doppler shifts less than 5%, and in most cases less than 1%, are typical. For example, a Mach 1 target (approximately 330 m/sec) at 10 GHz imparts a 22,000 Hz Doppler shift. For a 1 MHz bandwidth waveform, the fractional Doppler shift is 2.2%.

20.10.4 Spectral Interpretation of Range-Doppler Coupling

An examination of the LFM waveform's spectrum provides insight into the range-Doppler coupling and Doppler tolerance observed in the previous section. Consider the LFM spectrum defined in equation (20.55) and repeated here for convenience

$$X(\omega) \approx |X(\omega)| \exp\left(-j\frac{1}{4\pi}\frac{\tau}{B}\omega^2\right)\exp\left(j\frac{\pi}{4}\right) \tag{20.89}$$

where $|X(\omega)| \approx 1, -\pi B \leq \omega \leq \pi B$. For a waveform $x(t)$, the Doppler-shifted signal may be modeled as $x(t)\exp(j\omega_d t)$ where $\omega_d = 2\pi f_d$. The Fourier transform of $x(t)\exp(j\omega_d t)$ is

$$x(t)\exp(j\omega_d t) \overset{\mathfrak{F}}{\longleftrightarrow} X(\omega - \omega_d) \tag{20.90}$$

The spectrum of a Doppler-shifted LFM waveform is then

$$X(\omega - \omega_d) \approx |X(\omega - \omega_d)| \exp\left(-j\frac{1}{4\pi}\frac{\tau}{B}(\omega - \omega_d)^2\right)\exp\left(j\frac{\pi}{4}\right) \tag{20.91}$$

Applying a filter matched at zero Doppler yields the output spectrum $X(\omega - \omega_d)H(\omega)$:

$$\begin{aligned} Y(\omega) = {} & |X(\omega - \omega_d)| \exp\left(-j\frac{1}{4\pi}\frac{\tau}{B}(\omega - \omega_d)^2\right)\exp\left(j\frac{\pi}{4}\right) \\ & \times |X(\omega)| \exp\left(j\frac{1}{4\pi}\frac{\tau}{B}\omega^2\right)\exp\left(-j\frac{\pi}{4}\right) \end{aligned} \tag{20.92}$$

or

$$Y(\omega) \approx |X(\omega - \omega_d)||X(\omega)| \exp\left(j\frac{1}{4\pi}\frac{\tau}{B}2\omega \cdot \omega_d\right) \exp\left(j\frac{1}{4\pi}\frac{\tau}{B}\omega_d^2\right) \tag{20.93}$$

Substituting $\omega_d = 2\pi f_d$ yields

$$Y(\omega) \approx |X(\omega - 2\pi f_d)||X(\omega)| \exp\left(j\frac{f_d}{B}\tau\omega\right) \exp\left(j\frac{1}{4\pi}\frac{\tau}{B}(2\pi f_d)^2\right) \tag{20.94}$$

The coupling between range and Doppler is a result of the linear phase term in equation (20.94), which produces a time delay at the output of the filter equal to $-f_d\tau/B$.

Given that $|X(\omega)| \approx 1, -\pi B \leq \omega \leq \pi B$ for large time-bandwidth products, the magnitude response may be approximated as

$$|Y(\omega)| \approx |X(\omega - \omega_d)||X(\omega)| \approx \begin{cases} 1, & -\pi(B - f_d) \leq \omega \leq \pi B,\ f_d > 0 \\ 1, & -\pi B \leq \omega \leq \pi\,(B + f_d)\,,\ f_d < 0 \\ 0, & \text{otherwise} \end{cases} \tag{20.95}$$

The mismatch between the filter and Doppler shifted waveform yields a composite spectrum with reduced bandwidth approximately equal to $B - |f_d|$, which translates into degraded range resolution. The composite spectrum also contains less energy, which translates into a loss in peak amplitude.

In the frequency domain, the LFM waveform's quadratic phase produces a linear phase term in (20.94) that governs range-Doppler coupling. A waveform possessing a higher-order phase response will produce in the presence of uncompensated Doppler additional terms that degrade the compressed response. Thus, the LFM is unique in terms of its Doppler tolerance.

20.10.5 Dealing with Doppler Modulation in a Pulse Compression Waveform

In a radar system, Doppler shift and its impact on a waveform may be dealt with in several ways:

1. With a priori knowledge, waveform modulations and parameters may be selected to achieve a Doppler-tolerant waveform for the anticipated range of Doppler shifts. The ambiguity function is an essential tool supporting this type of analysis and design.
2. In some cases, a bank of matched filters may be employed—each one tuned to a different Doppler shift. The Doppler spacing between filters is based on the tolerance of the waveform. The received signal is passed through each filter, and the filter yielding the largest response is the one that most closely matches the received waveform in both time delay and Doppler.
3. A target's radial velocity may be estimated during track or via some other means. The velocity estimate may be used to center the received signal at baseband by applying a frequency shift to the transmit or receive waveform. Only a single Doppler shift (or target) may be compensated for at a time. Differences between the actual Doppler shift and the estimated frequency shift represent an uncompensated Doppler component. The impact of uncompensated Doppler must be considered in the design.

20.10.6 The V-LFM

The accuracy with which a radar is required to measure range is dependent on the function being performed. For example, in some cases range accuracy is less important in search than in track. In search, a higher degree of range-Doppler coupling may be acceptable. The transition from search to track requires one to consider techniques for estimating and compensating for Doppler. Rihaczek [34] describes a V-LFM waveform that consists of both an up-chirp and down-chirp segment. The up-chirp gives a time displacement of the target response equal to $-(f_d/B)\tau$, whereas the down-chirp gives a displacement in the opposite direction equal to $+(f_d/B)\tau$. The ambiguity surface consists of two sheared ridges with opposite slopes. A variant on the V-LFM uses two pulses closely spaced in time (one up-chirp and one down-chirp) to resolve the range-Doppler ambiguity and to estimate the observed Doppler shift. The estimated Doppler shift may then be applied as one transitions to track to compensate for Doppler. In track, the range-rate estimate is continually updated and may be applied to the next pulse to compensate for Doppler.

20.11 LFM SUMMARY

The LFM waveform has been in use since the 1950s and possesses some unique properties. The waveform exhibits a linear relationship between time and frequency and is known for its Doppler tolerance and sheared ridge ambiguity surface. In high-resolution systems, stretch processing [15] is often applied to an LFM waveform to reduce the processing bandwidth while maintaining the resolution afforded by the transmit bandwidth. The LFM waveform may also be applied in search and track. In this text, the waveform was used to introduce a number of general concepts including matched filter implementations, ambiguity surfaces, processing gain, sidelobe suppression, and Doppler tolerance.

20.12 PHASE-CODED WAVEFORMS

Phase codes form a second broad class of pulse compression waveforms. Phase-coded waveforms are composed of concatenated subpulses (or *chips*) where the phase sequencing or coding from subpulse to subpulse is chosen to elicit a desired mainlobe and sidelobe response. Waveform properties are largely dependent on the coding sequence employed, and both biphase- and polyphase-coded waveforms are used in modern radar systems.

20.12.1 The Structure and General Properties of Phase-Coded Waveforms

Phase-coded waveforms are constructed of concatenated subpulses or "chips." A chip of duration τ_{chip} is illustrated in Figure 20-22. A rectangular-shaped chip has a Rayleigh resolution defined by

$$\delta R = \frac{c\tau_{chip}}{2} \tag{20.96}$$

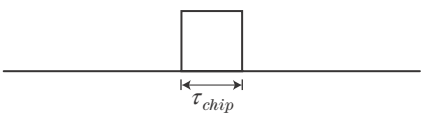

FIGURE 20-22 ■ A phase coded waveform consists of a set of concatenated sub-pulses or chips each of duration τ_{chip}.

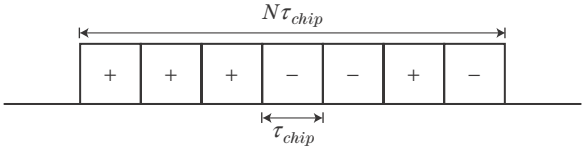

FIGURE 20-23 ■ Biphase coded waveforms consist of chips exhibiting 2 possible phase states.

and exhibits a sinc-shaped spectrum with a −4 dB bandwidth given by

$$B_{chip} = \frac{1}{\tau_{chip}} \tag{20.97}$$

Within a single chip, range resolution and waveform energy are inversely coupled. Increasing the chip width degrades resolution and increases the energy in the chip, while the converse occurs if the chip width is decreased.

Phase-coded waveforms are formed by concatenating N chips and selecting the phase of each chip to achieve a desired mainlobe and sidelobe response at the output of the corresponding matched filter. A baseband, biphase-coded waveform is illustrated in Figure 20-23. The allowable phase states, ϕ, are 0 and 180 degrees, and the chip amplitudes are defined by evaluating $\exp(j\phi)$ yielding either 1 or −1, respectively. The energy in a phase-coded waveform is proportional to the total pulse duration, τ, where

$$\tau = N\tau_{chip} \tag{20.98}$$

Appropriately chosen phase codes yield a Rayleigh range resolution defined by equation (20.96). Figure 20-24 contains a plot of the magnitude of the match filtered response associated with the phase code in Figure 20-23. The response has been normalized by the sequence length resulting a peak value of 1 and peak sidelobes of 1/7 (approximately 0.143). Using the Rayleigh criterion to define resolution, the distance between the mainlobe peak and first null is equal to the chip width.

The sidelobes in Figure 20-24 were achieved without amplitude weighting. The selection and ordering of the phase sequence determines the shape of the sidelobe response. This is in contrast to an LFM waveform where amplitude weighting facilitates sidelobe suppression but at a cost of degraded resolution and a loss in SNR.

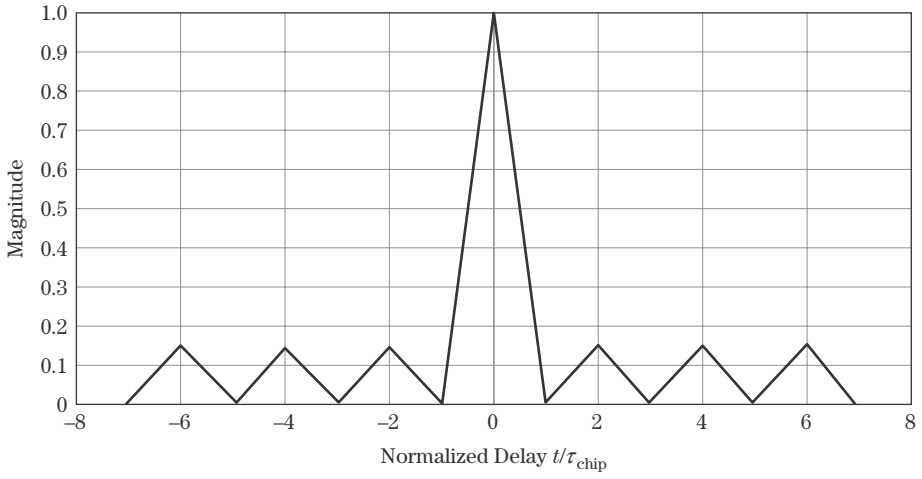

FIGURE 20-24 ■ Match filtered response for the Barker phase coded waveform (Figure 20-23) maintains equal peak sidelobes of level 1/N.

Phase-coded waveforms are compressed by applying a matched filter to the receive waveform. The filter may be implemented in the digital domain using fast convolution (see Section 20.8). The ADCs in Figure 20-12 are required to sample at a rate equal to or greater than the chip rate.

The time-bandwidth product associated with a phase-coded waveform is given by

$$\tau B = \tau B_{chip} = \frac{\tau}{\tau_{chip}} = N \tag{20.99}$$

and is equal to the number chips in the sequence. As with a frequency modulated waveform, the time-bandwidth product defines the gain in SNR at the output of the matched filter.

Phase codes are desired that exhibit low time sidelobes to meet both peak and integrated requirements. In general, sidelobe levels are inversely proportional to the sequence length. Long sequences may also be needed to satisfy SNR requirements, since the energy in a phase-coded waveform is proportional to the waveform duration $N\tau_{chip}$. As the chip duration is reduced to improve range resolution, energy in the waveform is decreased for a fixed length code. Thus, long codes may be needed to meet both the sidelobe and SNR requirements of a waveform.

20.12.2 Phase Codes Used in Radar

Selection of a phase code is based on a number of factors including the sidelobe response and sequence length. Optimal codes providing the minimum peak sidelobe (MPS) for a given sequence length have been identified for both biphase and polyphase codes [2,7,19–24,35–41]. These include the Barker codes, which achieve a 1:N peak sidelobe to mainlobe ratio. Biphase MPS codes have been identified through length 105 [22]. However, a requirement exists, in some cases, for longer sequences with predictable sidelobe levels. Nested codes are constructed by modulating one biphase code with another (e.g., Barker codes) to produce a code whose length is equal to the product of the two code lengths and whose peak sidelobe is defined by the longer of the two sequence lengths [7]. A *maximum length sequence* (MLS) is a biphase code of length $2^n - 1$ where n is an integer. The peak sidelobes of an MLS are inversely proportional to the square root of the sequence length [25,26].

Polyphase codes have the potential to exhibit lower sidelobes than a biphase code of equal length. Examples of polyphase codes with predictable sidelobe levels are the Frank, P1, and P2 codes [42,43]. Doppler tolerant polyphase codes include the P3 and P4 codes [27]. Quadriphase codes are polyphase codes designed to reduce the spectral energy located outside the nominal waveform bandwidth [28]. Spectral leakage represents a potential source of electromagnetic interference.

As with frequency modulated waveforms, mismatched filters may also be applied to a phase code to shape the sidelobe response [44–48]. Mismatched filters are used to reduce both the integrated and peak sidelobes as well as to tailor the sidelobe response in a given region.

The previous list is not meant to be comprehensive but includes some of the more common waveforms. Other phase codes are described in [2,4,6–8]. This chapter focuses on the MPS, MLS, Frank, P1, P2, P3, and P4 codes.

20.12.3 Phase Modulation

Phase-coded waveforms are partitioned into two categories: biphase and polyphase. Biphase-coded waveforms restrict their phase states to two values (e.g., 0° and 180°). Polyphase-coded waveforms exhibit more than two phase states (e.g., 0°, 90°, 180°, and 270°). The code sequence a_n is obtained by evaluating the complex exponential

$$a_n = \exp(j\phi_n) \quad n = 0, \ldots, N-1 \tag{20.100}$$

where ϕ_n is the phase (in radians) applied to the n-th chip. A biphase code consisting of phase states $\{0°, 180°\}$ yields a code sequence consisting of elements $\{1, -1\}$. A phase-coded waveform is represented either in terms of its phase sequence expressed in degrees or radians or in terms of the complex or real sequence defined by evaluating equation (20.100). In some cases, biphase codes are expressed in terms of 0's and 1's instead of -1's and 1's, respectively. The conversion from $\{0, 1\}$ to $\{-1, 1\}$ is performed by multiplying the sequence by 2 and subtracting 1.

On transmit, a phase-coded waveform is mixed to an RF. An expression for the RF signal is

$$x_{RF}(t) = \cos\left\{2\pi f_c t + \phi_n \left[u\left(t - (n)\,\tau_{chip}\right) - u\left(t - (n+1)\,\tau_{chip}\right)\right]\right\} \quad 0 \le t \le \tau, 0 \le n \le N-1 \tag{20.101}$$

where $u(t)$ is a unit step function. For example, given the sequence $\{1\ \ 1\ \ 1\ -1\ -1\ -1\ \ 1\ -1\ -1\ \ 1\ -1\}$, the baseband and RF modulated signals are shown in Figure 20-25. Note that the RF phase transitions occur at chip boundaries (denoted by asterisks) corresponding to a change or transition in the code sequence. A transition in the code sequence from 1 to -1 or from -1 to 1 corresponds to a 180° phase change.

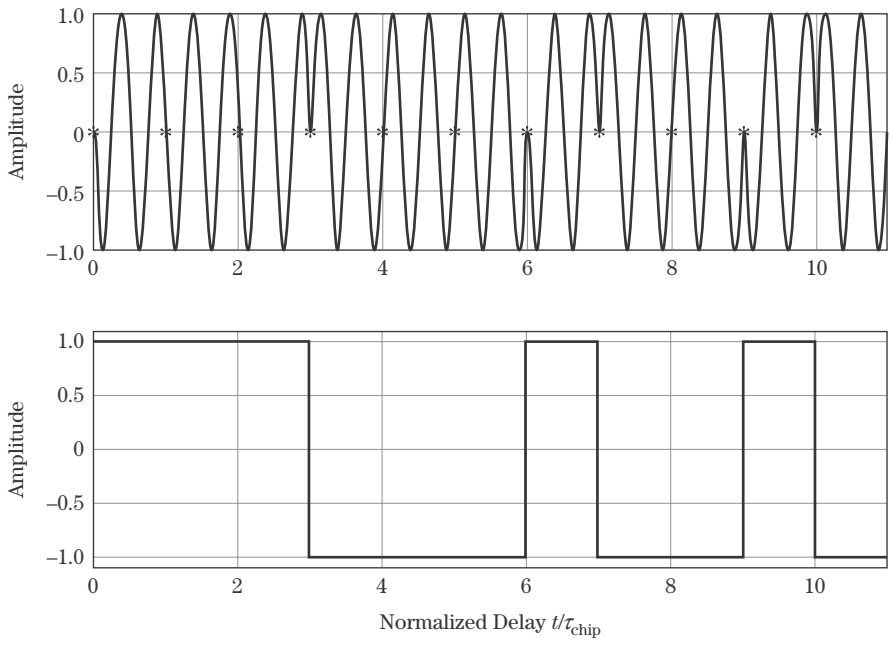

FIGURE 20-25 ■ Baseband (bottom) and RF modulated (top) phase coded waveform of length $N = 11$.

From a hardware perspective, biphase codes may be easier to implement than polyphase codes. However, with the advent of digital waveform generators, polyphase codes are just as likely to be used in a modern radar system as biphase codes. In general, polyphase-coded waveforms may be designed to achieve lower sidelobe levels than a biphase code of the same length. A polyphase code possesses more degrees of freedom (i.e., possible phase states), and these additional degrees of freedom may be exploited to achieve lower sidelobes. In addition, some polyphase codes are Doppler tolerant.

20.12.4 Equivalence Operations

Phase codes exhibiting identical match filtered magnitude responses are defined to be *equivalent*. Four operations may be applied to a code to generate an equivalent code. The magnitude response is preserved under the following operations [7]:

$$\hat{a}_n = a_{N-n}$$

$$\hat{a}_n = a_N^*$$

$$\hat{a}_n = \rho a_n, \text{ where } |\rho| = 1$$

$$\hat{a}_n = \rho^n a_n, \text{ where } |\rho| = 1$$

where $\hat{a}_n$ is an equivalent code and ρ is a unit-amplitude complex number.

20.12.5 Match Filtered Response of a Phase Code

A matched filter is applied to a phase-coded waveform to compress the waveform in range and maximize SNR. Consider the three chip sequence depicted in Figure 20-26 and the corresponding match filtered response in Figure 20-27. The response is obtained

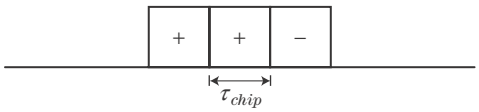

FIGURE 20-26 ■ Three chip Barker biphase code.

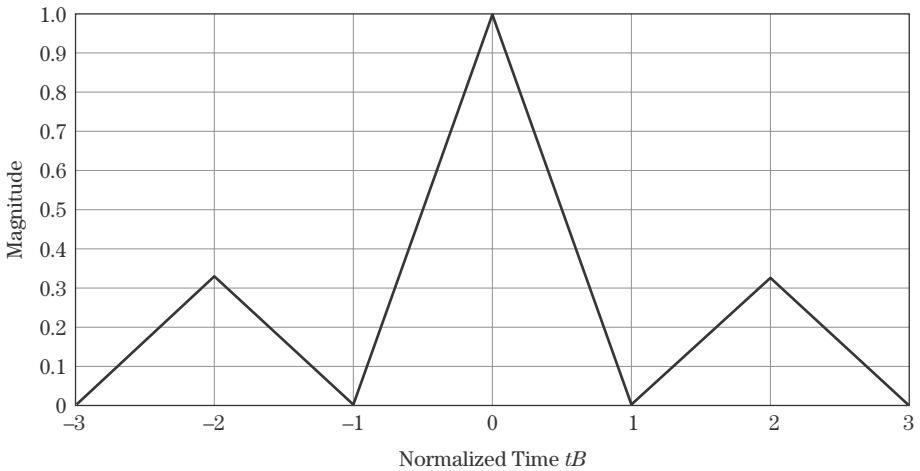

FIGURE 20-27 ■ The compressed response of the Barker code (Figure 20-26) has two equal sidelobes of $1/3$.

by correlating the sequence $\{1, 1, -1\}$ with itself. Normalizing the sequence to unit energy (i.e., $\{1/\sqrt{3}, 1/\sqrt{3}, -1/\sqrt{3}\}$), the peak of the response is equal to 1, and the peak sidelobe has a value of $1/3$. Note that the output of the filter is interpreted as a voltage. Thus, the sidelobe-to-peak ratio is $1{:}N$ in voltage and $1{:}N^2$ in power. The abscissa in Figure 20-27 represents time delay and is normalized by the chip width. The Rayleigh resolution occurs at a time delay corresponding to the chip width. For a rectangular-shaped chip, the Rayleigh resolution also corresponds to the -6 dB width.

As noted previously, both the peak and integrated sidelobes are important performance metrics. Ignoring the affects of band-limiting, the peak and integrated sidelobes may be examined using the code sequence and ignoring the chip response. The phase code's autocorrelation sequence is defined as

$$y[k] = \sum_{n=0}^{N-1} a_n a_{n-k}^* \quad k = -(N-1), \ldots, 0, \ldots (N-1) \tag{20.102}$$

and is equivalently obtained by sampling the waveform's match filtered response at multiples of the chip width. The ISR may be computed from the autocorrelation response and is defined as

$$ISR = \frac{2\sum_{k=1}^{N-1} |y[k]|^2}{N^2} \tag{20.103}$$

For the response in Figure 20-27, the ISR is 2/9, or -6.5 dB.

20.12.6 Spectrum of a Phase-Coded Waveform

The spectrum of a phase-coded waveform differs significantly from that of an LFM or NLFM waveform; however, properties associated with a phase-coded waveform may also be inferred from its spectrum. A derivation and examination of the spectrum of a phase-coded waveform is presented.

A phase-coded waveform $x(t)$ may be modeled in the time domain as

$$x(t) = \sum_{n=0}^{N-1} a_n p(t - n\tau_{chip}) \tag{20.104}$$

where an individual chip $p(t)$ is a unit amplitude rectangle defined by

$$p(t) = 1 \quad -\frac{\tau_{chip}}{2} \le t \le \frac{\tau_{chip}}{2} \tag{20.105}$$

and $\{a_n\}$ is the code sequence. For biphase codes, $a_n \in \{1, -1\}$, and for polyphase codes $a_n \in \mathbb{C}$ where $\mathbb{C}$ represents the set of unit-amplitude complex numbers. For the waveform in equation (20.104), $t = 0$ is referenced to the center of the first chip. The Fourier transform of the waveform is

$$X(\omega) = P(\omega) \sum_{n=0}^{N-1} a_n \exp(-j\omega n\tau_{chip}) \tag{20.106}$$

where $P(\omega)$ is the Fourier transform of a single chip centered at $t = 0$. The time offset to each chip, $n\tau_{chip}$, appears in the frequency domain as the argument of a complex exponential. The spectrum consists of the product of the chip spectrum $P(\omega)$ and the DTFT of the phase sequence.

To compress the chip sequence, a matched filter is applied to the waveform spectrum. The matched filter was defined in Section 20.2.3 as $x^*(-t)$ in the time domain or $X^*(\omega)$ in the frequency domain. Applying $X^*(\omega)$ to $X(\omega)$ yields

$$Y(\omega) = |P(\omega)|^2 \sum_{n=0}^{N-1} a_n \exp(-j\omega n \tau_{chip}) \sum_{m=0}^{N-1} a_m^* \exp(j\omega m \tau_{chip}) \tag{20.107}$$

or

$$Y(\omega) = |P(\omega)|^2 C(\omega) \tag{20.108}$$

where

$$C(\omega) = \sum_{m=0}^{N-1} \sum_{n=0}^{N-1} a_n a_m^* \exp(-j\omega \tau_{chip}(n-m)) \tag{20.109}$$

The composite spectrum consists of the product of the magnitude-squared of the chip's spectrum and the double summation in equation (20.109), which is a function of the code sequence. The double summation may be expressed as

$$C(\omega) = \sum_{k=-(N-1)}^{N-1} c_k \exp(-j\omega k \tau_{chip}) \tag{20.110}$$

where c_k is defined as

$$c_k = \sum_{m=k}^{N-1-k} a_{m-k} a_m^* \quad 0 \le k \le (N-1) \tag{20.111}$$

and

$$c_{-k} = c_k^* \tag{20.112}$$

The sequence c_k, in (20.111), represents the discrete autocorrelation of the code sequence, and $C(\omega)$ represents its DTFT.

The spectral components $C(\omega)$ and $P(\omega)$ are plotted in Figure 20-28 for the sequence $\{1, 1, -1\}$ and a rectangular chip. The spectrum of the chip is a sinc function. In the composite spectrum, $P(\omega)$ is modulated by $C(\omega)$, yielding $Y(\omega)$. A plot of the composite power spectrum is provided in the lower subplot of Figure 20-28. In general, the spectrum of a phase-coded waveform resembles a "noisy" or amplitude modulated sinc.

The shape of the compressed response is a function of both the coding sequence and the compressed chip response. The compressed response $y(t)$ may be written in terms of delayed and weighted copies of the filtered chip response $y_{chip}(t)$ where

$$y(t) = \sum_{k=-(N-1)}^{N-1} c_k y_{chip}(t - k\tau_{chip}) \tag{20.113}$$

and the chip response is obtained by taking the inverse Fourier transform of the chip spectrum

$$y_{chip}(t) = \frac{1}{2\pi} \int_{-\infty}^{\infty} |P(\omega)|^2 \exp(j\omega t) d\omega \tag{20.114}$$

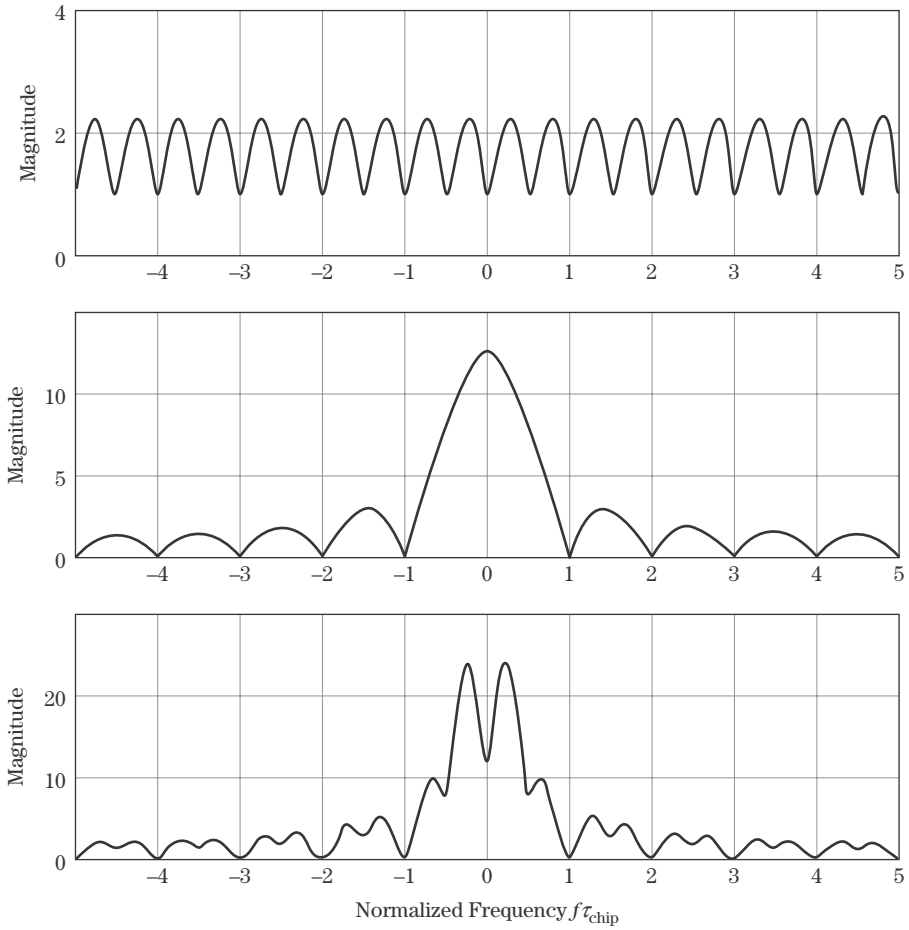

FIGURE 20-28 ■ Top: Spectrum of the 3 bit phase code $C(\omega)$. Middle: Chip spectrum $P(\omega)$. Bottom: Composite spectrum $Y(\omega)$. See text for details.

The match filtered response is encoded in both the time and frequency domains. As an example, consider the three-chip sequence in Figure 20-26. For this sequence, the double summation in equation (20.110) becomes

$$\sum_{k=-(N-1)}^{N-1} c_k \exp(-j\omega k\tau_{chip}) = -e^{j\omega 2\tau_{chip}} + 3 - e^{-j\omega 2\tau_{chip}} \tag{20.115}$$

The filtered spectrum is then given by

$$Y(\omega) = -|P(\omega)|^2 e^{j\omega 2\tau_{chip}} + 3|P(\omega)|^2 - |P(\omega)|^2 e^{-j\omega 2\tau_{chip}} \tag{20.116}$$

The spectrum of a rectangular chip is a sinc, and the inverse transform of a squared sinc is a triangle. The compressed response therefore consists of three weighted triangles centered at time delays $t = \{-2\tau_{chip}, 0, 2\tau_{chip}\}$ as illustrated in Figure 20-27. Note that the match filtered spectrum $Y(\omega) = X(\omega)X^*(\omega) = |X(\omega)|^2$ is real and that $Y(\omega) \geq 0$. The spectrum in (20.116) is thus real and may be written as

$$Y(\omega) = -2|P(\omega)|^2 \cos(\omega 2\tau_{chip}) + 3|P(\omega)|^2 \tag{20.117}$$

The spectra associated with frequency modulated waveforms often have relatively simple shapes, for example, the approximate rectangular shape of an LFM waveform's spectrum. As a result, it is often easy to predict the match filtered time-domain response from the spectral shape. In contrast, the spectra of phase-coded waveforms have more complex shapes, making it difficult if not impossible to predict the match filtered time-domain response from the spectrum. For phase-coded waveforms, an autocorrelation is required to determine the time-domain response.

Band-limiting modifies the chip's spectrum and thus the composite spectrum. Filters in the transmitter and receiver increase the duration of a chip resulting in cross-talk, which degrades the sidelobe response and reduces bandwidth resulting in degraded resolution. The level of degradation depends on the degree of band-limiting imposed. The impact of band-limiting is illustrated in Section 20.14.2 using a Frank and P1 code.

In most instances, phase-code waveform properties are assessed assuming no band-limiting (i.e., no filtering of the ideal chip response). In these cases, an assessment of sidelobe performance may be performed using the code sequence and ignoring the chip response.

20.12.7 Doppler Tolerance

Doppler tolerance refers to the degree of degradation in the compressed response due to uncompensated Doppler. As discussed in Section 20.10.3, an LFM waveform is characterized as Doppler tolerant, exhibiting range-Doppler coupling and a preservation of the mainlobe and sidelobe response over large fractional Doppler shifts. Biphase-coded waveforms are considered to be *Doppler intolerant* when the residual Doppler exceeds one-quarter cycle over the uncompressed pulse length.

In the absence of a Doppler shift, the mainlobe of a phase code achieves its maximum at $k = 0$ in equation (20.111). In the presence of a Doppler shift f_d, the response at $k = 0$ is

$$c_0 = \frac{1}{N}\sum_{m=0}^{N-1} \exp(j2\pi f_d m \tau_{chip}) \tag{20.118}$$

for a unit energy phase code. Applying the finite sum formula, (20.118) reduces to

$$|c_0| = \frac{1}{N}\left|\frac{\sin(N\pi f_d \tau_{chip})}{\sin(\pi f_d \tau_{chip})}\right| \tag{20.119}$$

This quantity is zero when $f_d = 1/N\tau_{chip}$, which is equivalent to one full cycle of Doppler over the uncompressed pulse. One-quarter cycle of Doppler produces 1 dB of peak loss, and one-half cycle produces 4 dB of loss.

Doppler also causes each chip's phase to rotate, degrading the sidelobe response. A half-cycle of Doppler causes a phase change of 180° between the first and last chip. In general, biphase codes are designed to experience no more than a quarter-cycle of uncompensated Doppler. A quarter-cycle limits the degradation in the sidelobe response and corresponds to a 1 dB loss in SNR.

Some polyphase codes exhibit a Doppler tolerance similar to that of an LFM waveform, but not all polyphase codes are Doppler tolerant. In most cases, Doppler tolerance is an issue only when employing long pulses or in the presence of large Doppler shifts. If the Doppler shift is known or has been estimated, it may be removed through processing

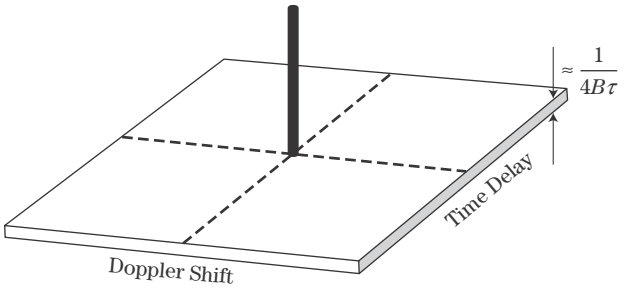

FIGURE 20-29 ■ The ambiguity surface associated with some phase coded waveforms is a thumb tack.

or modulation prior to the matched filter. In addition, a bank of matched filters may be employed, as described in Section 20.10.5.

In general, biphase codes do not exhibit range-Doppler coupling. In some cases, the ambiguity surface resembles a thumbtack [30,34]. A thumbtack ambiguity surface exhibits a narrow impulse-like response centered at zero Doppler and delay and a low plateau response extending over the waveform bandwidth in Doppler and pulse width in delay, as illustrated in Figure 20-29. Some biphase-coded waveforms exhibit large responses in the plateau region that are above the nominal sidelobe levels [30] and thus diverge from a thumbtack response.

A waveform possessing a thumbtack-like ambiguity surface may be used to simultaneously estimate a target's range and Doppler shift by employing a bank of filters, each matched to a different Doppler shift. The filter exhibiting the largest response is associated with the target's true range and Doppler.

The ambiguity surface associated with a polyphase code may resemble a thumbtack, a sheared ridge, or some other shape. The P3 and P4 polyphase codes [27] examined in Section 20.14.3 exhibit range-Doppler coupling and a Doppler tolerance similar to an LFM waveform.

20.13 BIPHASE CODES

Biphase codes have been identified that exhibit low, predictable sidelobe levels and in some cases achieve the minimum peak sidelobe for a given code length. Codes commonly applied in radar systems include Barker codes, MPS codes, and maximal length sequences [2,7,19–24,25–26].

20.13.1 Biphase Barker Codes

Biphase Barker codes exhibit a peak sidelobe to mainlobe voltage ratio of $1{:}N$, where N is the code length. The peak sidelobe ratio is defined in terms of power and is expressed as $20\log_{10}(1/N)$. The Barker codes achieve the lowest possible PSR for an aperiodic code. The known biphase Barker codes are listed in Table 20-4 with their corresponding peak sidelobe ratios. Equivalent codes are obtained using the transforms defined in Section 20.12.4.

The longest known Barker code is length 13 with a corresponding peak sidelobe ratio of -22.3 dB. Figure 20-30 contains a plot of the compressed response for a 13-bit Barker with unit energy. The peak sidelobe is $1/13 \approx 0.077$. It has been shown [4] that no odd-length biphase Barker sequence exists longer than length 13. No even-length sequences

TABLE 20-4 ■ A List of the Known Biphase Barker Codes

Code Length	Code Sequence	Peak Sidelobe Level, dB
2	+−, ++	−6.0
3	++−	−9.5
4	++−+, +++−	−12.0
5	+++−+	−14.0
7	+++−−+−	−16.9
11	+++−−−+−−+−	−20.8
13	+++++−−++−+−+	−22.3

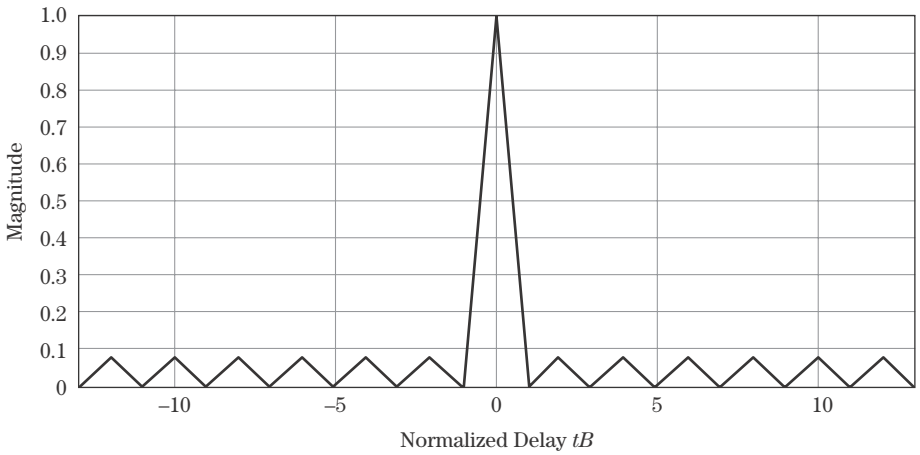

FIGURE 20-30 ■ Compressed response for the longest Barker biphase code: 13 chips.

have been found above length 4, and it can be shown that if a longer even-length sequence does exist, the sequence length must be a perfect square [4].

20.13.2 MPS codes

Given the length limitations of Barker codes, longer sequences with low peak sidelobe ratios are desired. Searches have been performed to identify biphase codes that yield MPS ratios for a given sequence length. Lindner [21] identified MPS codes up to length 40. Excluding the Barker codes, these MPS codes exhibit peak sidelobe ratios of either 2:N or 3:N in voltage. Codes with an MPS ratio equal to 2:N exist for lengths 6, 8–10, 12, 14–21, 25, and 28, while codes with an MPS ratio equal to 3:N exist for lengths 22–24, 26, 27, and 29–40. The number of MPS codes per sequence length varies significantly from 1 code for a 13-bit Barker code to 858 MPS codes for a 24-length sequence. Cohen et al. [19] developed techniques for judiciously searching for MPS codes and extended the known MPS codes to lengths 41 through 48. The MPS codes of length 41–48 exhibit peak sidelobe ratios of 3:N. Figure 20-31 contains the compressed response for a 48-length biphase MPS code with a −24.08 dB peak sidelobe.

Kerdock et al. [20] identified an MPS code of length 51 with a peak sidelobe ratio of 3:N, and Coxson and Russo [22] and Coxson et al. [24] extended the list of known MPS codes to include lengths 49, 50, and 52–70 with a peak sidelobe ratio of 4:N. Nunn and Coxson [23] conjectured, given the current body of evidence, that no sequence greater than length 51 exhibits a peak sidelobe ratio of 3:N or less. They added to the list of codes exhibiting a peak sidelobe ratio of 4:N to lengths of 71–82 and the list of those exhibiting a

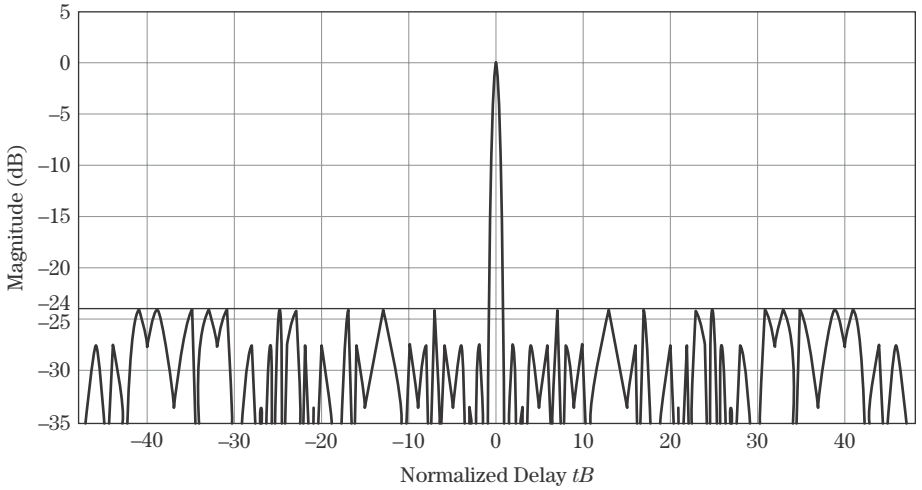

FIGURE 20-31 ■ Compressed response for a 48-length Minimal Peak Sidelobe (MPS) code achieves a 3:48 peak sidelobe ratio.

TABLE 20-5 ■ Summary of MPS Code Lengths and Corresponding Peak Sidelobe Levels

Peak Sidelobe Level (Voltage)	Code Length
1	2–5, 7, 11, 13
2	6, 8–10, 12, 14–21, 25, 28
3	22–24, 26, 27, 29–40, 41–48, 51
4	49, 50, 52–70, 71–82
5	83–105

peak sidelobe ratio of 5:N to lengths of 83–105. The searches were not exhaustive, but the codes achieve the best MPS ratio known to date for these code lengths. Table 20-5 contains a summary of MPS code lengths and their corresponding peak sidelobe levels. Cohen et al. [19] provides example MPS codes that also exhibit the lowest integrated sidelobe level. Cohen et al.'s list and other example MPS codes through length 105 [19–24] are provided in Table 20-6.[1] The number of codes identified for a given code length is also provided in Table 20-6. The count does not include equivalent codes obtained using the operations in Section 20.12.5.

20.13.3 Maximal Length Sequences

The biphase MPS codes, which include the Barker codes, achieve the lowest peak sidelobe for a given sequence length; however, in many radar applications an optimum code is not required given that a "good" code with relatively low sidelobe levels is available. Biphase maximum length sequences are used in radar applications and provide predictable peak sidelobe ratios that approach $10\log_{10}(1/N)$. Maximum length sequences are binary sequences whose pattern of 1's and -1's does not repeat within a period equal to $2^n - 1$, where n is an integer. MLSs are generated using a shift register

$$s_i = a_1 s_{i-1} \oplus a_2 s_{i-2} \oplus \ldots \oplus a_n s_{i-n} \qquad i = 1, \ldots, 2^n - 1 \tag{20.120}$$

[1]Note that the 103-length code is incorrect in [23] due to a typographical error. The corrected code was supplied by Carroll Nunn and is provided in Table 20-6.

TABLE 20-6 ■ Example Biphase MPS Codes through Length 105

Code Length	Peak Sidelobe	Number of Codes	Example Code (Hexadecimal)
2	1	1	2
3	1	1	6
4	1	1	D
5	1	1	1D
6	2	4	0B
7	1	1	27
8	2	8	97
9	2	10	D7
10	2	5	167
11	1	1	247
12	2	16	9AF
13	1	1	159F
14	2	9	1483
15	2	13	182B
16	2	10	6877
17	2	4	774B
18	2	2	190F5
19	2	1	5BB8F
20	2	3	5181B
21	2	3	16BB83
22	3	378	E6D5F
23	3	515	38FD49
24	3	858	64AFE3
25	2	1	12540E7
26	3	242	2380AD9
27	3	388	25BBB87
28	2	2	8F1112D
29	3	283	164A80E7
30	3	86	2315240F
31	3	251	2A498C0F
32	3	422	3355A780
33	3	139	CCAA587F
34	3	51	333FE1A55
35	3	111	796AB33
36	3	161	3314A083E
37	3	52	574276F9E
38	3	17	3C34AA66
39	3	30	13350BEF3C
40	3	57	2223DC3A5A
41	3	15	38EA520364
42	3	4	4447B874B4
43	3	12	5B2ACCE1C
44	3	15	FECECB2AD7
45	3	4	2AF0CC6DBF6
46	3	1	3C0CF7B6556
47	3	1	69A7E851988
48	3	4	156B61E64FF3
49	4	Not Reported	012ABEC79E46F
50	4	Not Reported	025863ABC266F
51	3	Not Reported	71C077376ADB4
52	4	Not Reported	0945AE0F3246F
53	4	Not Reported	0132AA7F8D2C6F

TABLE 20-6 ■ (*Continued*)

Code Length	Peak Sidelobe	Number of Codes	Example Code (Hexadecimal)
54	4	Not Reported	0266A2814B3C6F
55	4	Not Reported	04C26AA1E3246F
56	4	Not Reported	099BAACB47BC6F
57	4	Not Reported	01268A8ED623C6F
58	4	Not Reported	023CE545C9ED66F
59	4	Not Reported	049D38128A1DC6F
60	4	Not Reported	0AB8DF0C973252F
61	4	Not Reported	005B44C4C79EA350
62	4	Not Reported	002D66634CB07450
63	4	Not Reported	04CF5A2471657C6F
64	4	1859	55FF84B069386665
65	4	Not Reported	002DC0B0D9BCE5450
66	4	Not Reported	0069B454739F12B42
67	4	Not Reported	007F1D164C62A5242
68	4	Not Reported	009E49E3662A8EA50
69	4	Not Reported	0231C08FDA5A0D9355
70	4	Not Reported	1A133B4E3093EDD57E
71	4	Not Reported	63383AB6B452ED93FE
72	4	Not Reported	E4CD5AF0D054433D82
73	4	Not Reported	1B66B26359C3E2BC00A
74	4	Not Reported	36DDBED681F98C70EAE
75	4	Not Reported	6399C983D03EFDB556D
76	4	Not Reported	DB69891118E2C2A1FA0
77	4	Not Reported	1961AE251DC950FDDBF4
78	4	Not Reported	328B457F0461E4ED7B73
79	4	Not Reported	76CF68F327438AC6FA80
80	4	Not Reported	CE43C8D986ED429F7D75
81	4	Not Reported	0E3C32FA1FEFD2519AB32
82	4	Not Reported	3CB25D380CE3B7765695F
83	5	Not Reported	711763AE7DBB8482D3A5A
84	5	Not Reported	CE79CCCDB6003C1E95AAA
85	5	Not Reported	19900199463E51E8B4B574
86	5	Not Reported	3603FB659181A2A52A38C7
87	5	Not Reported	7F7184F04F4E5E4D9B56AA
88	5	Not Reported	D54A9326C2C686F86F3880
89	5	Not Reported	180E09434E1BBC44ACDAC8A
90	5	Not Reported	3326D87C3A91DA8AFA84211
91	5	Not Reported	77F80E632661C3459492A55
92	5	Not Reported	CC6181859D9244A5EAA87F0
93	5	Not Reported	187B2ECB802FB4F56BCCECE5
94	5	Not Reported	319D9676CAFEADD68825F878
95	5	Not Reported	69566B2ACCC8BC3CE0DE0005
96	5	Not Reported	CF963FD09B1381657A8A098E
97	5	Not Reported	1A843DC410898B2D3AE8FC362
98	5	Not Reported	30E05C18A1525596DCCE600DF
99	5	Not Reported	72E6DB6A75E6A9E81F0846777
100	5	Not Reported	DF490FFB1F8390A54E3CD9AAE
101	5	Not Reported	1A5048216CCF18F83E910DD4C5
102	5	Not Reported	2945A4F11CE44FF664850D182A
103	5	Not Reported	77FAA82C6E065AC4BE18F274CB
104	5	Not Reported	E568ED4982F9660EBA2F611184
105	5	Not Reported	1C6387FF5DA4FA325C895958DC5

Sources: Compiled from [19–24].

TABLE 20-7 ■ Coefficients for an Irreducible, Primitive Polynomial through Order 13

Degree of Polynomial	Coefficients (Octal)	Coefficients (Binary)
2	7	111
3	13	1011
4	23	10011
5	45	100101
6	103	1000011
7	211	10001001
8	435	100011101
9	1021	1000010001
10	2011	10000001001
11	4005	100000000101
12	10123	1000001010011
13	20033	10000000011011

employing feedback where $\{s_i, s_{i-1}, \ldots, s_{i-n}\}$ are the individual shift registers, each containing either a 0 or a 1. The operator $\oplus$ denotes modulo 2 addition. The feedback coefficients d_k, $k = 1, \ldots, n$, are obtained from the coefficients of an irreducible, primitive polynomial

$$h(x) = d_n x^n + d_{n-1} x^{n-1} + \cdots + d_1 x + 1 \tag{20.121}$$

where the coefficients d_k are either 0 or 1 and are equal to the shift register coefficients of (20.120), $d_n = a_n$. Cook [4] defines a primitive polynomial as one that divides evenly into $x^m + 1$ where $m > 2^n - 1$. Irreducible, primitive polynomials of degree n exists for all values of n [25], and Peterson [49] provides tables of primitive irreducible polynomials up to order 34. More than one irreducible polynomial may exist for a given order. Table 20-7 contains the coefficients for a single, primitive irreducible polynomial through order 13.

Figure 20-32 contains a shift register configured to generate a 31-length MLS. The sequence is obtained by recording the output of any one of the shift registers. The shift registers are initialized with a sequence of 1's and 0's, excluding the all-zero condition. The compressed response for a 127-length MLS is provided in Figure 20-33 and exhibits a peak sidelobe of approximately -21 dB. Note that the sidelobes are very low near the mainlobe and increase away from the mainlobe approaching the predicted peak sidelobe level before rolling off at the ends. This shape is characteristic of the compressed response associated with an MLS.

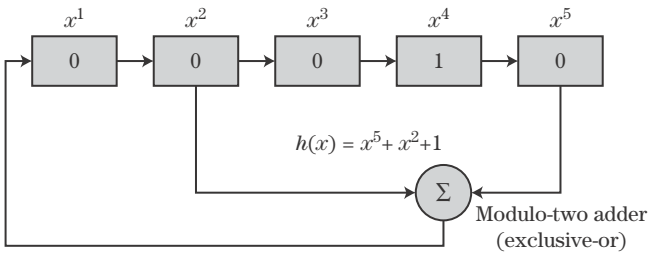

FIGURE 20-32 ■ A shift register employing feedback generates a 31-length Maximal Length Sequence.

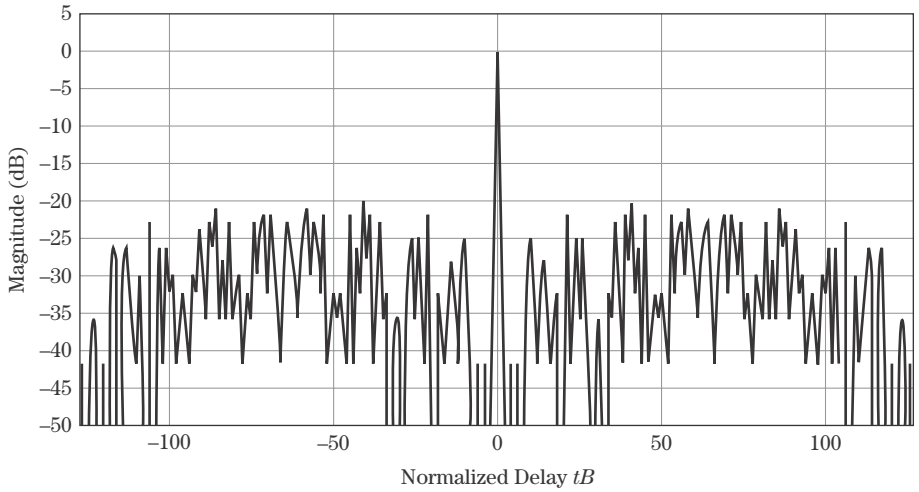

FIGURE 20-33 ■ The compressed response for a 127-length MLS.

20.13.4 Comparison of MLS and LFM Waveform Responses and Spectra

In general, the sidelobe structure of the match filtered response for a biphase-coded waveform is relatively uniform, whereas the sidelobes of a frequency modulated waveform roll-off with range. Figure 20-34 contains the compressed response for an MLS with a time-bandwidth product of 1,023 (gray curve) and an unweighted LFM waveform with a time-bandwidth product of 1,000 (black curve). The peak sidelobe ratio for the LFM waveform and MLS are −13.2 dB and −28.6 dB, respectively. The sidelobe roll-off associated with the LFM waveform and the more constant response associated with the MLS are evident. The ISR for the LFM waveform and MLS were calculated to be −9.7 dB and −4.8 dB, respectively. The relatively flat sidelobe response associated with the phase-coded waveform yields a higher ISR even though the peak sidelobe is much lower. An LFM weighted with a −30 dB Taylor and a TB of 1,000 yields an ISR of −22 dB. The roll-off of the sidelobes associated with a frequency modulated waveform aids in reducing the integrated sidelobe ratio.

Frequency modulated waveforms exhibit a compact spectral support in comparison with most phase-coded waveforms. Figure 20-35 contains a plot of the spectrum of a

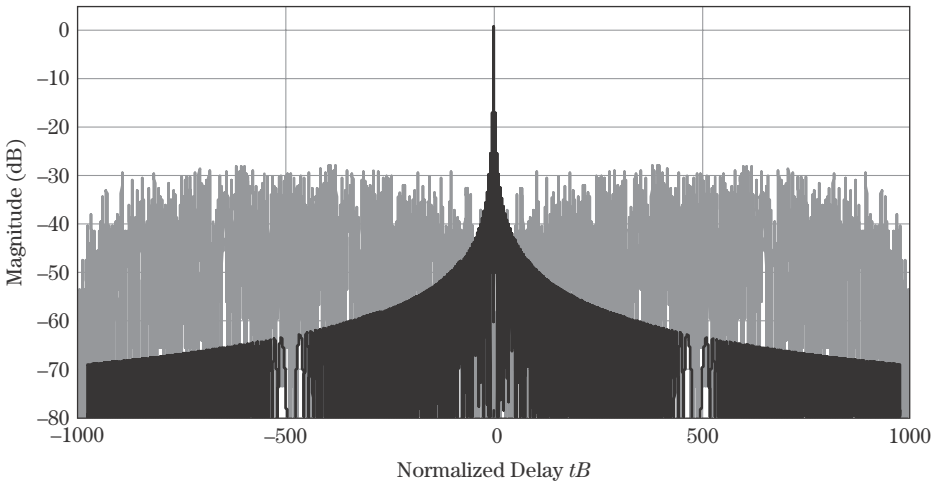

FIGURE 20-34 ■ Comparison of a compressed LFM waveform (black curve) (TB = 1000) with a compressed biphase MLS coded waveform (gray curve) (TB = 1023).

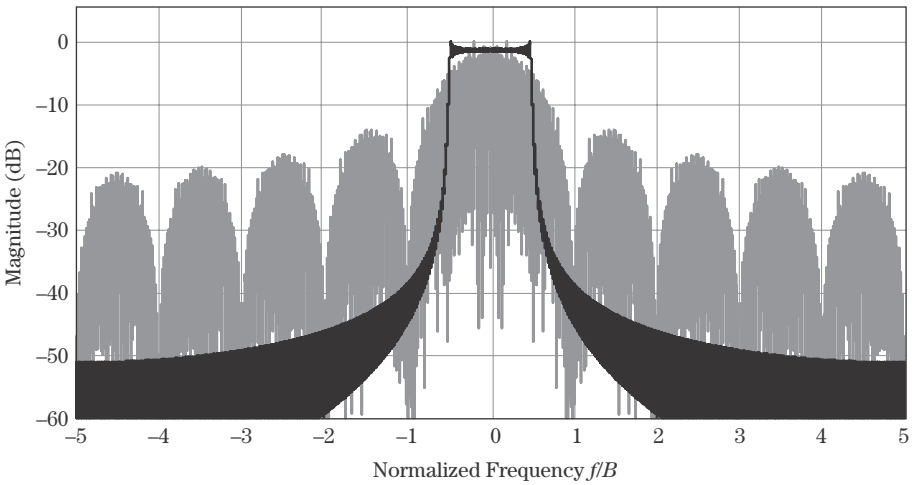

FIGURE 20-35 ■ Comparison of the spectra of an LFM waveform (black curve) with a 1023-length MLS coded waveform (gray curve).

biphase-coded waveform derived from a 1,023-length MLS with a 10 nanosecond chip width. The spectrum of the phase-coded waveform resembles a "noisy" sinc function. Overlaid on the MLS is the spectrum of an LFM waveform with a 100 MHz bandwidth. The phase-coded waveform exhibits a significant amount of energy outside the nominal 100 MHz bandwidth. This out-of-band energy is a potential source of *electromagnetic interference* (EMI) for a system operating nearby in frequency and in close physical proximity. Quadriphase codes and chip shaping have been used to reduce the energy located outside the nominal waveform bandwidth [7,28].

20.14 POLYPHASE CODES

Polyphase-coded waveforms possess more than two phase states and offer the potential for Doppler tolerance similar to that of an LFM waveform as well as lower peak sidelobes for a given length code. Polyphase Barker, Frank, P1, P2, P3, and P4 codes are examined in the following sections.

20.14.1 Polyphase Barker Codes

Polyphase Barker codes [35–41] exhibiting a peak sidelobe ratio of $1{:}N$ have been identified employing various search techniques. The phases are either unrestricted or restricted to a P-th root of unity such that the allowable phase increment is $\Delta\phi = 2\pi/P$ and P is an integer greater than 2. Borweinan and Ferguson [36] have identified polyphase Barker codes up to length 63. Several of the codes extracted from [36] are provided in Table 20-8. The compressed response associated with a 45-length polyphase Barker sequence is provided in Figure 20-36 with a theoretical peak sidelobe of -33.06 dB. Nunn and Coxson [39] have recently identified polyphase Barker codes of length 64–70 and 72, 76, and 77.

20.14.2 Frank, P1, and P2 Codes

Frank codes [42,43] are polyphase codes with a phase sequence defined by

$$\phi_{n,k} = \frac{2\pi}{M} nk \qquad n, k = 0, \ldots, (M-1) \tag{20.122}$$

TABLE 20-8 ■ Example Polyphase Barker Codes Where $\phi_n = 2\pi p_n / P$

Code Length, N	P	$p_n, n = 1, \ldots, N$
63	2,000	0, 0, 88, 200, 250, 89, 1832, 1668, 1792, 145, 308, 290, 528, 819, 1357, 1558, 1407, 1165, 930, 869, 274, 97, 10, 1857, 731, 789, 1736, 150, 1332, 1229, 390, 944, 1522, 1913, 648, 239, 1114, 1708, 200, 666, 1870, 1124, 1464, 265, 845, 1751, 1039, 53, 737, 1760, 798, 1880, 851, 1838, 1103, 419, 1711, 1155, 546, 1985, 1325, 754, 44
60	210	0, 0, 16, 208, 180, 153, 126, 161, 135, 78, 83, 98, 143, 127, 162, 153, 183, 141, 72, 207, 149, 167, 15, 13, 146, 58, 23, 109, 169, 208, 75, 143, 173, 199, 51, 50, 31, 142, 152, 84, 74, 6, 147, 205, 151, 66, 51, 151, 27, 101, 170, 75, 172, 91, 20, 131, 1, 78, 166, 68
57	240	0, 0, 18, 51, 31, 37, 6, 39, 43, 64, 128, 167, 187, 19, 22, 226, 163, 103, 97, 238, 200, 172, 111, 201, 72, 95, 75, 172, 2, 91, 49, 220, 209, 57, 212, 168, 116, 206, 110, 102, 25, 131, 2, 30, 143, 182, 42, 107, 216, 89, 10, 161, 29, 170, 106, 205, 86
54	200	0, 0, 23, 43, 16, 9, 40, 51, 20, 7, 67, 126, 178, 180, 71, 120, 144, 151, 61, 25, 45, 100, 86, 9, 172, 161, 142, 22, 85, 8, 96, 128, 81, 1, 18, 137, 0, 95, 132, 59, 44, 155, 16, 129, 157, 98, 47, 174, 73, 18, 145, 65, 170, 100
51	50	0, 0, 4, 4, 18, 20, 27, 25, 25, 26, 24, 15, 15, 14, 9, 32, 36, 2, 21, 17, 9, 27, 46, 49, 19, 29, 9, 32, 7, 45, 21, 46, 22, 47, 18, 35, 0, 22, 9, 31, 44, 5, 29, 21, 4, 49, 33, 24, 9, 49, 29

Source: Extracted from [36].

where the phase, $\phi_{n,k}$, is indexed over n for each value of k. The length of the code, N, is required to be a perfect square, $N = M^2$. The peak sidelobe ratio in dB [50] is $20\log_{10}\{1/[N\sin(\pi/M)]\}$ for N even and $20\log_{10}\{1/[2N\sin(\pi/2M)]\}$ for N odd. The upper plot in Figure 20-37 contains the compressed response for a 100-length Frank code. The peak sidelobe ratio is approximately -30 dB. Note that a biphase 127-length MLS would yield a PSR of approximately -21 dB. The additional degrees of freedom in the polyphase code support a lower PSR for nearly the same length code.

Frank codes exhibit range-Doppler coupling similar to an LFM waveform but are Doppler intolerant, exhibiting high near-in sidelobes in the presence of small fractional

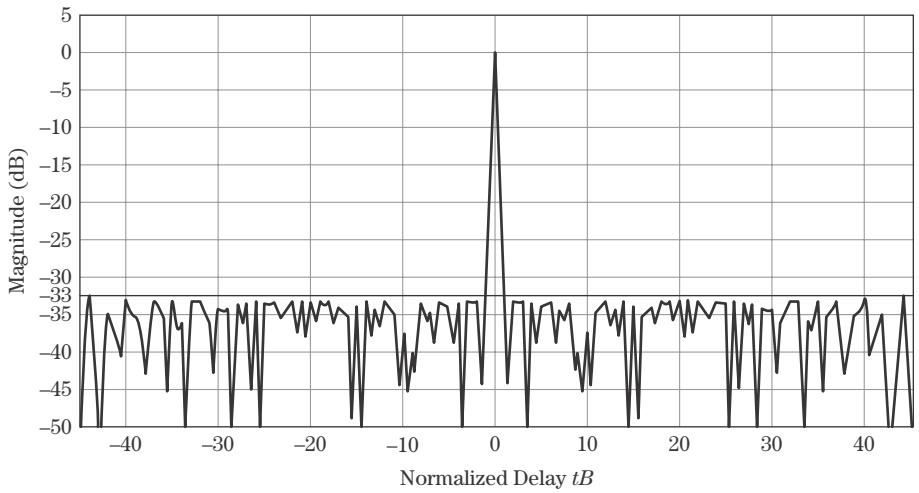

FIGURE 20-36 ■ The compressed response for a 45-length polyphase Barker code achieves a 1:45 peak sidelobe ratio.

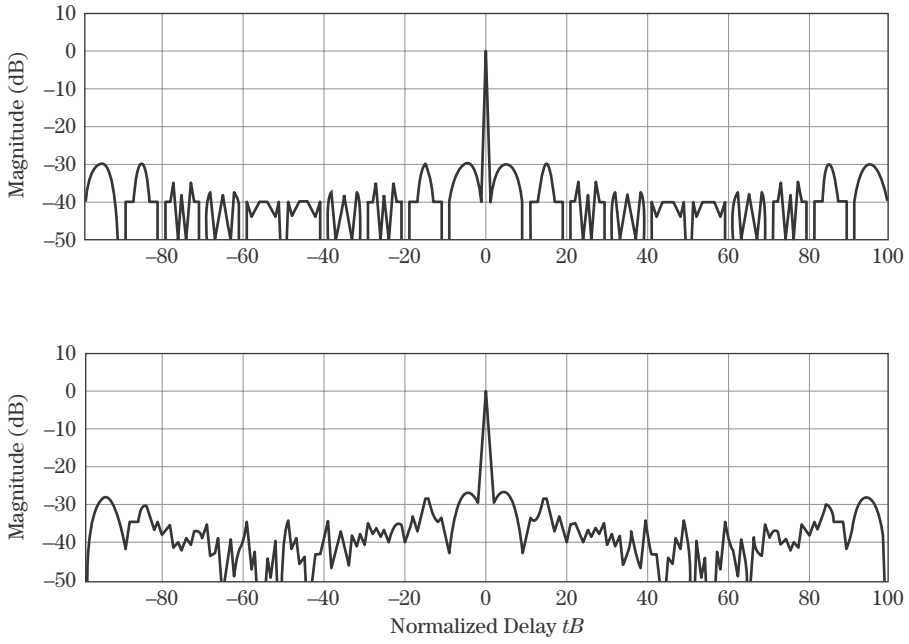

FIGURE 20-37 ■ The compressed response for a 100-length Frank code with no bandlimting (upper plot) and with bandlimiting (lower plot).

Doppler shifts. Figure 20-38 contains the compressed response associated with a 100-length Frank code with one cycle of Doppler across the uncompressed pulse. The mainlobe is displaced by one resolution cell, and the peak sidelobe has increased by approximately 11 dB.

Band-limiting causes the peak sidelobes of a Frank code to increase above their nominal level. Figure 20-39 contains a plot of the spectrum of a 100-length Frank code and the frequency response of a 20th-order finite impulse response filter. In this example, the filter's −6 dB width is equal to the waveform bandwidth ($B = 1/\tau_{chip}$). Figure 20-37 contains a plot of the autocorrelation with and without filtering. Careful examination reveals that the peak sidelobes have increased from −29.8 dB to −28.2 dB, an increase of 1.6 dB. Lewis and Kretschmer [51] describe the Frank code as exhibiting a slow phase

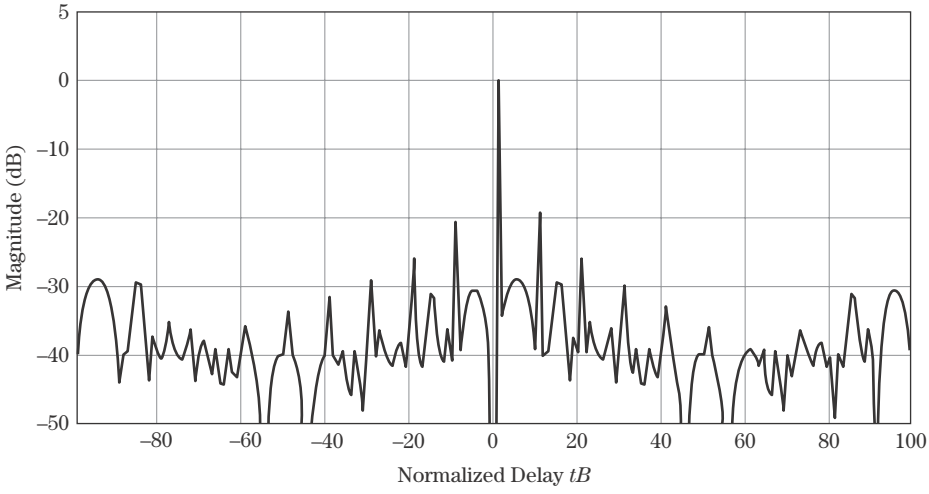

FIGURE 20-38 ■ The matched filter response for a 100-length Frank code with one cycle of Doppler over the uncompressed pulse.

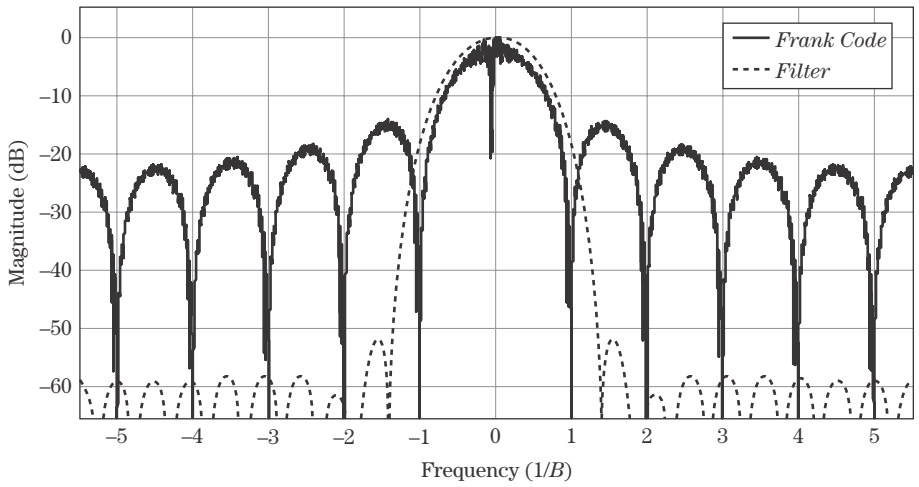

FIGURE 20-39 ■ Spectrum of a 100-length Frank code and a 20th order finite impulse response filter.

variation at the ends of the code and a faster phase variation near the middle of the code. The filter performs a smoothing operation [7] that integrates the slower varying phase terms producing the increased sidelobes near the end of the code. Band-limiting also broadens the mainlobe, which degrades resolution.

To address the impact of band-limiting, Lewis and Kretschmer [51] developed the P1 and P2 codes. The codes are designed to exhibit better sidelobe performance in the presence of band-limiting. The phase sequence defining a P1 code is

$$\phi_{n,k} = -\frac{\pi}{M}(M - 2k - 1)(Mk + n), \quad n = 0, \ldots, (M-1), k = 0, \ldots, (M-1) \tag{20.123}$$

and the phase sequence defining a P2 code is

$$\phi_{n,k} = \frac{\pi}{2M}(M - (2n+1))(M - 2k), \quad n = 0, \ldots, (M-1), k = 0, \ldots, (M-1) \tag{20.124}$$

where the phase, $\phi_{n,k}$, is indexed over n for each value of k. Either even or odd values of M may be used for the P1 code. For the P2 code, M is required to be even to achieve low sidelobes. In contrast to the Frank code, the P1 and P2 codes exhibit a slow phase variation in the center of the code and a faster phase variation at the ends. The modification is intended to reduce the effects of band-limiting on the sidelobe structure. Figure 20-40 contains the autocorrelation response for a P1 code with and without filtering. The sidelobes associated with the filtered sequence in Figure 20-40 are lower than those depicted in Figure 20-37. This is particularly evident near the ends of the autocorrelation response.

The magnitude of the P1 code's autocorrelation response is identical to that of the Frank code. The peak sidelobes of the P2 match the Frank code, and the magnitude of the autocorrelation response approaches that of the Frank code as the time-bandwidth product is increased. For M odd, the ambiguity surface of a P1 code is identical to that of Frank code. For M even, the P1 and P2 ambiguity surfaces are similar to the ambiguity surface associated with a Frank code [51].

20.14.3 P3 and P4 Codes

The Doppler intolerance of the Frank, P1, and P2 codes led Lewis and Kretschmer [27] to develop the P3 and P4 codes, which exhibit a Doppler tolerance similar to that of an

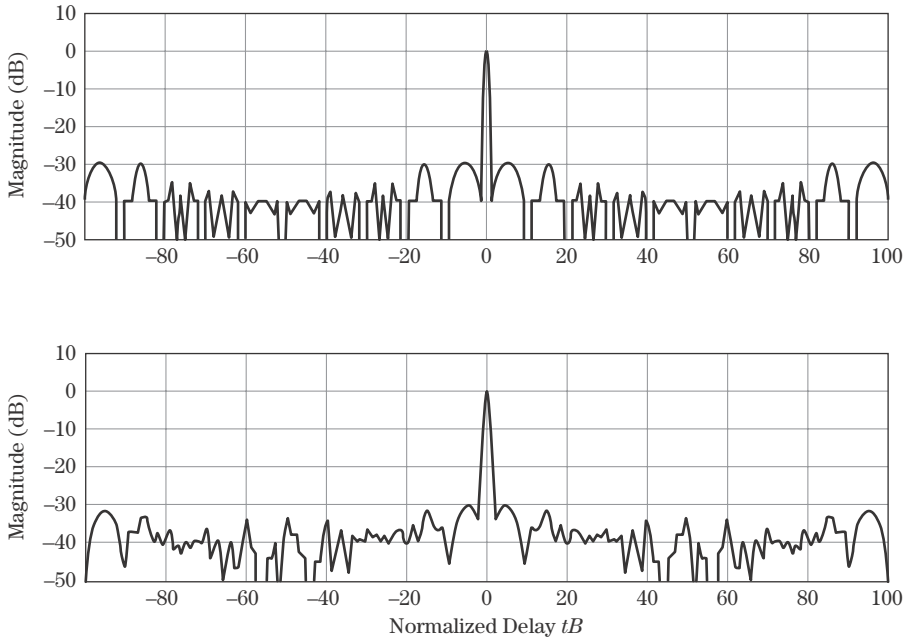

FIGURE 20-40 ■ The compressed response for a 100-length P1 code with no bandlimting (upper plot) and with bandlimiting (lower plot).

LFM waveform. The P3 and P4 codes are derived by sampling the quadratic phase of an LFM waveform. Consider an LFM waveform

$$x(t) = \exp\left(j\pi \frac{B}{\tau} t^2\right), \quad 0 \le t \le \tau \tag{20.125}$$

Sampling the phase in (20.125) at the chip interval τ_{chip} yields the phase sequence

$$\phi_n = \frac{\pi B}{\tau}(n\tau_{chip})^2 \tag{20.126}$$

For a rectangular chip, the chip width is the reciprocal of the bandwidth, $\tau_{chip} = 1/B$. Making the appropriate substitutions, the phase code in (20.126) reduces to

$$\phi_n = \frac{\pi}{N} n^2 \quad n = 0, \ldots, (N-1) \tag{20.127}$$

where N is the sequence length. The phase sequence in (20.127) defines a P3 code. The ambiguity surface for a P3 code is similar to that of an LFM waveform and does not exhibit the higher near-in sidelobes associated with Frank, P1, and P2 codes in the presence of small fractional Doppler shifts.

The P4 code is designed to be both Doppler tolerant and to perform well in the presence of precompression band-limiting. The P4 code's phase sequence is

$$\phi_n = \frac{\pi}{N} n^2 - \pi n \quad n = 0, \ldots, (N-1) \tag{20.128}$$

For large time-bandwidth products, the peak sidelobe ratio of the P3 and P4 codes [7] is approximately $10\log_{10}(2.5/\pi^2 N)$, which is about 4 dB higher than those associated with the same length Frank code. Figure 20-41 contains a plot of the match filtered response for a 100-length P4 code. Note that the peak sidelobes are approximately 4 dB higher than the Frank code response in Figure 20-37 (upper plot).

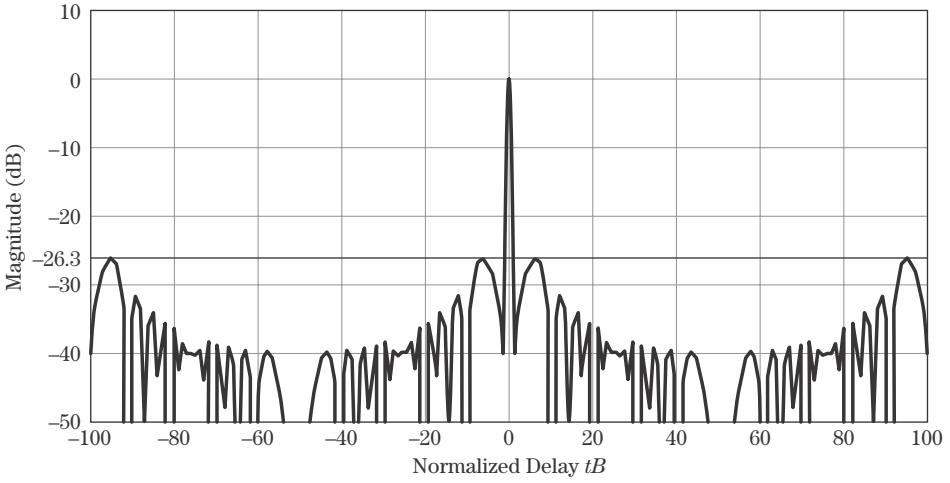

FIGURE 20-41 ■ The match filtered response for a 100-length P4 code.

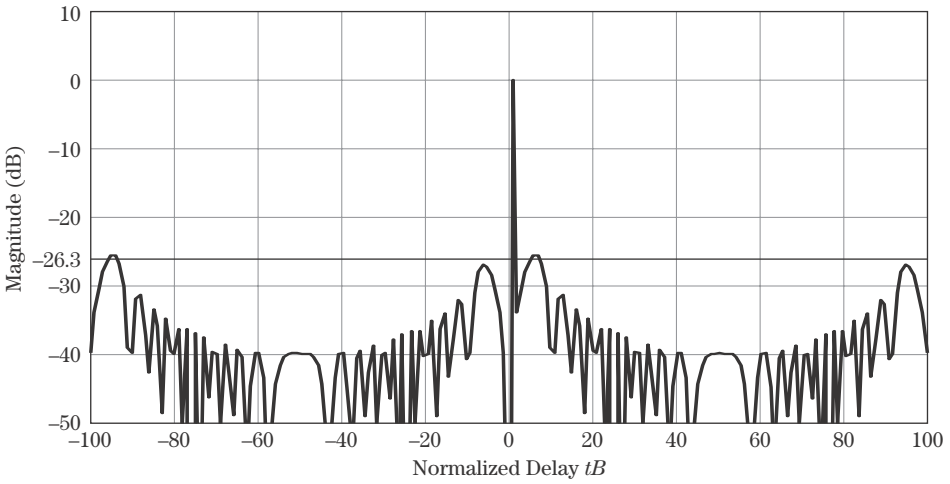

FIGURE 20-42 ■ The matched filter response for a 100-length P4 code with one cycle of Doppler over the uncompressed pulse length.

The Doppler tolerance of the P4 code relative to that of the Frank code is shown by comparing the responses in Figure 20-42 and Figure 20-38. Figure 20-42 contains the match filtered response for a P4 with a single cycle of Doppler across the uncompressed pulse. The effect of the Doppler shift is a displacement of the mainlobe by one resolution cell and a slight increase in the peak sidelobes. Figure 20-38 contains the match filtered response for a Frank of the same length with a single cycle of Doppler across the uncompressed pulse. The Frank code exhibits range-Doppler coupling similar to a P4 code, but the near-in sidelobes increase dramatically. The peak sidelobe has increased by ≈ 11 dB compared with ≈ 1 dB for the P4 code.

20.15 PHASE-CODE SUMMARY

Phase codes are applied in many modern radar systems and decouple energy and resolution via chip-to-chip phase modulation. Range resolution is proportional to the chip width, and peak sidelobes are inversely related to the sequence length. Minimum peak sidelobe codes achieve the lowest sidelobe level for a given code length, but the longest known

biphase MPS codes are on the order of length 105. Longer codes with predictable, but not necessarily minimum, sidelobe ratios are available including the maximal length sequences. Biphase coded waveforms are designed to constrain the uncompensated Doppler to one-quarter cycle over of the pulse. This constraint limits the SNR loss and preserves the sidelobe structure. Polyphase codes, in many cases, achieve a lower sidelobe level for a given sequence length and in some cases may be designed to achieve a Doppler tolerance similar to an LFM waveform.

20.16 FURTHER READING

Books principally devoted to the theory and application of radar waveforms are few in a number. Cook and Bernfeld [4] and Rihaczek [34] are two older texts still in print, and, more recently, Levanon and Mozeson [7] have written an excellent text on the subject. Many modern radar texts [2, 6, 8, 52, 53] also provide a thorough discussion of pulse compression waveforms.

A number of phase and frequency modulated waveforms and techniques are covered in the literature and are worthy of further investigation including nonlinear frequency modulation [54–60], stretch processing [15], stepped frequency [16,17], stepped chirp [18,61–63], Costas frequency arrays [2,7], mismatched filters [44–48], complementary codes [64], nested codes [7], P(n,k) codes [65], and quadriphase codes [28]. In addition, Sarwate and Pursely [26] provide bounds on autocorrelation and cross-correlation performance for periodic and aperiodic codes.

20.17 REFERENCES

[1] DiFranco, J.V., and Rubin, W.L., *Radar Detection*, Prentice-Hall, Inc., Englewood Cliffs, NJ, 1968.

[2] Peebles Jr., P.Z., *Radar Principles*, John Wiley & Sons, Inc., New York, 1998.

[3] Turin, G.L., "An Introduction to Matched Filters," *IRE Transactions on Information Theory*, pp. 311–319, June 1960.

[4] Cook, C.E., and Bernfeld, M., *Radar Signals, An Introduction to Theory and Application*, Artech House, Boston, 1993.

[5] Woodward, P.M., *Probability and Information Theory, with Applications to Radar*, Artech House, Dedham, MA, 1980.

[6] Richards, M.A., *Fundamentals of Radar Signal Processing*, McGraw-Hill, New York, 2005.

[7] Levanon, N., and Mozeson, E., *Radar Signals*, Wiley, New York, 2004.

[8] Levanon, N., *Radar Principles*, John Wiley & Sons, New York, 1988.

[9] Papoulis, A., *The Fourier Integral and Its Applications*, McGraw-Hill, New York, 1987.

[10] Carrara, W.G., Goodman, R.S., and Majewski, R.M., *Spotlight Synthetic Aperture Radar, Signal Processing Algorithm*, Artech House, Boston, 1995.

[11] Novak, L.M., Halversen, S.D., and Owirka, G.J., "Effects of Polarization and Resolution on SAR ATR," *IEEE Transactions on Aerospace and Electronics Systems*, vol. 33, pp. 102–116, January 1997.

[12] Klauder, J.R., Price, A.C., Darlington, S., and Albersheim, W.J., "The Theory and Design of Chirp Radars," *Bell System Technical Journal,* vol. 34, pp. 745–808, July 1960.

[13] Kretschmer Jr., F.F., "Pulse Compression Waveforms Using Huffman Codes," *Proceedings of the 1986 IEEE National Radar Conference,* pp. 59–64, 1986.

[14] Huffman, D.A., "The Generation of Impulse-Equivalent Pulse Trains," *IRE Transactions on Information Theory*, vol. IT-8, pp. S10–S16, September 1962.

[15] Caputi Jr., W.J., "Stretch: A Time-Transformation Technique," *IEEE Transactions on Aerospace and Electronics Systems*, vol. AES-7, no. 2, pp. 269–278, March 1971.

[16] Wehner, D.R., *High Resolution Radar*, 2d ed., Artech House, Boston, 1995.

[17] Scheer, J.A. and Kurtz, J.L., *Coherent Radar Performance Estimation*, Artech House, Boston, 1993.

[18] McGroary, F., and Lindell, K., "A Stepped Chirp Technique for Range Resolution Enhancement," *IEE National Telesystems Conference*, pp. 121–126, 1991.

[19] Cohen, M.N., Fox, M.R., and Baden, J.M., "Minimum Peak Sidelobe Pulse Compression Codes," *Proceedings of the IEEE International Radar Conference,* Arlington, VA, pp. 633–638, May 7–10, 1990.

[20] Kerdock, A.M., Mayer, R., and Bass, D., "Longest Binary Pulse Compression Codes with Given Peak Sidelobe Levels," *Proceedings of the IEEE,* vol. 74, no. 2, p. 366, 1986.

[21] Lindner, J., "Binary Sequences Up to Length 40 with Best Possible Autocorrelation Function," *Electronic Letters,* vol. 11, no. 21, p. 507, October 1975.

[22] Coxson, G., and Russo, J., "Efficient Exhaustive Search for Optimal-Peak-Sidelobe Binary Codes," *IEEE Transactions on Aerospace and Electronic Systems,* vol. 41, no. 1, pp. 302–308, January 2005.

[23] Nunn, C.J., and Coxson, G.E., "Best-Known Autocorrelation Peak Sidelobe Levels for Binary Codes of Length 71-105," *IEEE Transactions on Aerospace and Electronic Systems,* vol. 44, no. 1, pp. 392–395, January 2008.

[24] Coxson, G.E., Hirschel, A., Cohen, M.N., "New Results on Minimum-PSL Binary Codes," *Proceedings of the 2001 IEEE Radar Conference,* pp. 153–156, 2001.

[25] MacWilliams, F.J., and Sloane, N.J.A., "Pseudo-Random Sequences and Arrays," *Proceedings of the IEEE,* vol. 64, no. 12, pp. 1715–1729, December 1976.

[26] Sarwate, D.V., and Pursley, M.B., "Crosscorrelation Properties of Pseudorandom and Related Sequences," *Proceedings of the IEEE,* vol. 68, no. 5, pp. 593–619, 1980.

[27] Lewis, B.L., and Kretschmer Jr., F.F., "Linear Frequency Modulation Derived Polyphase Pulse Compression Codes," *IEEE Transactions on Aerospace and Electronic Systems,* vol. 18, no. 5, pp. 637–641, September 1982.

[28] Taylor, J., and Blinchikoff, H., "Quadriphase Code—A Radar Pulse Compression Signal with Unique Characteristics," *IEEE Transactions on Aerospace and Electronic Systems,* vol. 24, no. 2, pp. 156–170, March 1988.

[29] Keel, B.M., and Heath, T.H., "A Comprehensive Review of Quasi-Orthogonal Waveforms," *2007 IEEE Radar Conference,* pp. 122–127, April 2007.

[30] Farnett, E.C., and Stevens, G.H., "Pulse Compression Radar," in *Radar Handbook,* 2d ed., Ed. M. Skolnik, McGraw-Hill, New York, 1990.

[31] Ludeman, L.C., *Fundamentals for Digital Signal Processing*, Harper & Row, New York, 1986.

[32] Blankenship, P.E., and Hofstetter, E., "Digital Pulse Compression via Fast Convolution," *IEEE Transactions on Acoustics, Speech, and Signal Processing*, vol. ASSP-23, no. 2, pp. 189–201, April 1975.

[33] Morris, G., and Harkness, L., *Airborne Pulsed Doppler Radar*, 2d ed., Artech House, Boston, 1996.

[34] Rihaczek, A.W., *Principles of High-Resolution Radar*, Artech House, Boston, 1996.

[35] Friese, M., and Zotman, H., "Polyphase Barker Sequences up to Length 31," *Electronic Letters,* vol. 30, no. 23, pp. 1930–1931, November 1994.

[36] Borwein, P., and Ferguson, R., "Polyphase Sequences with Low Autocorrelation," *IEEE Transactions on Information Theory,* vol. 51, no. 4, pp. 1564–1567, April 2005.

[37] Brenner, A.R., "Polyphase Barker Sequences up to Length 45 with Small Alphabets," *Electronic Letters,* vol. 34, no. 16, pp. 1576–1577, August 1998.

[38] Friese, M., "Polyphase Barker Sequences up to Length 36," *IEEE Transactions on Information Theory*, vol. 42, no. 4, pp. 1248–1250, July 1996.

[39] Nunn, C.J., and Coxson, G.E., "Polyphase Pulse Compression Codes with Optimal Peak and Integrated Sidelobes," *IEEE Transactions on Aerospace and Electronic Systems,* vol. 45, no. 2, pp. 775–781, 2009.

[40] Gartz, K.J., "Generation of Uniform Amplitude Complex Code Sets with Low Correlation Sidelobes," *IEEE Transactions on Signal Processing,* vol. 40, no. 2, pp. 343–351, February 1992.

[41] Bomer, L., and Antweiler, M., "Polyphase Barker Sequences," *Electronics Letters,* vol. 25, no. 23, pp. 1577–1579, 1989.

[42] Frank, R.L., "Polyphase Codes with Good Nonperiodic Correlation Properties," *IEEE Transactions on Information Theory,* vol. 9, pp. 43–45, January 1963.

[43] Lewis, B.L., Kretschmer Jr., F.F., and Shelton, W.W., *Aspects of Radar Signal Processing*, Artech House, Norwood, MA, 1986.

[44] Baden, J.M., and Cohen, M.N., "Optimal Sidelobe Suppression for Biphase Codes," *1991 IEEE National Telesystems Conference,* vol. 1, pp. 127–131, 1991.

[45] Baden, J.M., and Cohen, M.N., "Optimal Peak Sidelobe Filters for Biphase Pulse Compression," *Record of the IEEE 1990 International Radar Conference,* pp. 249–252, May 1990.

[46] Griep, K.R., Ritcey, J.A., and Burlingame, J.J., "Polyphase Codes and Optimal Filters for Multiple User Ranging," *IEEE Transactions on Aerospace and Electronics Systems*, vol. 31, pp. 752–767, April 1995.

[47] Zoraster, S., "Minimum Peak Range Sidelobe Filters for Binary Phase-Coded Waveforms," *IEEE Transactions on Aerospace and Electronic Systems,* vol. AES-16, no. 1, pp. 112–115, January 1980.

[48] Griep, K.R., Ritcey, J.A., and Burlingame, J.J., "Poly-Phase Codes and Optimal Filters for Multiple User Ranging," *IEEE Transactions on Aerospace and Electronic Systems,* vol. 31, no. 2, pp. 752–767, April 1995.

[49] Peterson, W.W., and Weldon Jr., E.J., *Error-Correcting Codes*, MIT Press, Cambridge, MA, 1972.

[50] Mow, W.H., and Li, S.R., "Aperiodic Autocorrelation and Crosscorrelation of Polyphase Sequences," *IEEE Transactions on Information Theory,* vol. 43, no. 3, pp. 1000–1007, May 1997.

[51] Lewis, B.L., and Kretschmer Jr., F.F., "A New Class of Polyphase Pulse Compression Codes and Techniques," *IEEE Transactions on Aerospace and Electronic Systems,* vol. 17, no. 3, pp. 364–372, May 1981.

[52] Nathanson, F.E., *Radar Design Principles*, 2d ed., McGraw-Hill, New York, 1991.

[53] Skolnik, M.I., *Introduction to Radar Systems*, 3d ed., McGraw Hill, New York, 2001.

[54] Johnston, J.A., and Fairhead, A.C., "Waveform Design and Doppler Sensitivity Analysis for Nonlinear FM Chirp Pulses," *IEE Proceedings–F,* vol. 133, no. 2, pp. 163–175, April 1986.

[55] Newton, C.O., "Nonlinear Chirp Radar Signal Waveforms for Surface Acoustic Wave Pulse Compression Filters," *Wave Electronics*, pp. 387–401, 1974.

[56] Johnston, J.A., "Analysis of the Pulse Compression of Doppler Shifted Nonlinear Frequency Modulated Signals," *Electronic Letters,* vol. 20, pp. 1054–1055, December 1984.

[57] Fowle, E.N., "The Design of FM Pulse Compression Signals," *IEEE Transactions on Information Theory,* pp. 61–67, January 1964.

[58] Brandon, M.A., "The Design of a Non-linear Pulse Compression System to Give a Low Loss High Resolution Radar Performance," *Marconi Review,* Vol. 36, no. 188, pp. 1–45, 1973.

[59] Brandon, M.A., "The Spectra of Linear and Non-linear F.M. Used in Pulse Compression, and the Effects on the Resultant Compressed Pulse," *Marconi Review,* Vol. 36, no. 188, pp. 69–92, 1973.

[60] Key, E.L., Fowle, E.N., Haggarty, R.D., "A Method of Designing Signals of Large Time-Bandwidth Product," *IRE International Convention Record,* vol. 9, pt. 4, pp. 146–154, 1961.

[61] Wilkinson, A.J., Lord, R.T., and Inggs, M.R., "Stepped-Frequency Processing by Reconstruction of Target Reflectivity Spectrum," *Proceedings of the 1998 South African Symposium on Communications and Signal Processing,* pp. 101–104, 1998.

[62] Lord, R.T., and Inggs, M.R., "High Range Resolution Radar using Narrowband Linear Chirps Offset in Frequency," *Proceedings of the 1997 South African Symposium on Communications and Signal Processing*, pp. 9–12, September 1997.

[63] Lord, R.T., and Inggs, M.R., "High Resolution SAR Processing Using Stepped-Frequencies," *1997 IEEE International Geoscience and Remote Sensing Conference,* pp. 490–492, August 1997.

[64] Golay, M., "Complementary Series," *IRE Transactions on Information Theory,* pp. 82–87, April 1960.

[65] Felhauer, T., "Design and Analysis of New P(n,k) Polyphase Pulse Compression Codes," *IEEE Transactions on Aerospace and Electronic Systems*, vol. 30, no. 3, pp. 865–874, July 1994.

20.18 PROBLEMS

1. Compute the Rayleigh range resolution associated with a simple, rectangular pulse with $\tau = 2$ μsec. Assume the speed of light $c = 3 \times 10^8$ m/sec and the amplitude of the pulse is unity. Sketch the ideal matched filtered response and label the time delay axis at the points $\{-\tau, -\tau/2, 0, \tau/2, \tau\}$ and the amplitude axis at the points $\{0, 0.5, 1\}$. Note that the filtered response represents a voltage. What dB value does the 0.5 amplitude value represent? What is the range resolution associated with the -3 dB width of the response? How does it compare with the Rayleigh resolution?

2. Given a waveform $x(t)$ and its Fourier transform $X(\omega)$, the waveform's matched filter $h(t)$ is defined as $h(t) = x^*(-t)$. Using the Fourier transform, derive the spectrum of the matched filter $H(\omega)$ in terms of $X(\omega)$.

3. Derive the matched filter for a waveform $x(t)$ embedded in white noise with power spectral density N_0. Show all of your work.

4. Compute the Fourier transform for a simple pulse defined by $x(t) = 1, -\tau/2 \leq t \leq \tau/2$. Show all of your work, and put the result in terms of a sinc response.

5. Given an LFM waveform with $B = 250$ MHz and $\tau = 2$ μsec, perform the following:

a. Compute the waveform time-bandwidth product.

b. In a baseband coherent detector, compute the minimum ADC rate required to support the waveform.

c. Given a 1 km range window, compute the minimum collection time to avoid eclipsing returns within the window.

d. Compute the number of complex samples obtained over the collection time in (c) given the sampling rate in (b).

e. Compute the pulse compression integration gain in dB. If the SNR prior to the matched filter is –3 dB, compute the SNR at the output of the matched filter.

6. Derive the matched filter response for an LFM waveform defined by $x(t) = \exp(j\pi(B/\tau)t^2)$ $-\tau/2 \leq t \leq \tau/2$. Show all of your work.

7. Derive the ambiguity function for the LFM waveform defined in problem 6.

8. Compute the Doppler shift required to displace an LFM with $B = 50$ MHz and $\tau = 1$ msec by 3 Rayleigh range resolution cells. At 10 GHz, compute the radial velocity associated with the Doppler shift.

9. Compute the integrated sidelobe ratios for the Barker codes in Table 20-4.

10. For the biphase code $\{1\ 1\ -1\ 1\}$, apply the four equivalence operations defined in Section 20.12.5 to the code. Assume $\rho = \exp(j\pi/4)$. In addition, apply the conjugate equivalence operation (third property) to the code generated by the fourth property. Show that each code possesses the same autocorrelation magnitude response.

11. Using the equivalence properties defined in Section 20.12.5, prove that any polyphase code may be written with the first two phase values equal to zero radians.

12. Given a 127 length MLS sequence and a pulse width equal to 2.54 μsec, compute the chip width, the waveform bandwidth, the Rayleigh range resolution, waveform time-bandwidth product, and the pulse compression gain (in dB). Compute the approximate peak sidelobe ratio associated with the phase-coded waveform. Compute the minimum Doppler shift required to annihilate the peak of the match filtered response.

13. Draw the shift register with feedback required to implement a 511 maximal length sequence. Use the polynomial coefficients defined in Table 20-7. Initialize the shift register, avoiding the all-zeros condition. Select an output register, and compute the first four values generated by the shift register. Convert this sequence of 0's and 1's to a sequence of 1's and -1's.

14. Compute the peak sidelobe ratio associated with the following waveforms: 13 chip biphase Barker code, 69 chip poly-phase Barker code, 144 and 169 length P1 codes, a 1,023 length MLS sequence, and a 102 length MPS code.

15. Design a phase-coded waveform for a pulsed radar to meet all of the following requirements:

a. Rayleigh range resolution $= 0.3$ meters.

b. Pulse compression gain > 15 dB.

c. Peak sidelobe ≤ -20 dB.

d. Maximum allowable blind range within the first range ambiguity $= 50$ meters.

e. Biphase-coded waveform.